

Polarized macrophages modulate cardiac structure and contractility under hypoxia in novel immuno-heart on a chip

Cite as: APL Bioeng. 9, 026114 (2025); doi: 10.1063/5.0253888

Submitted: 19 December 2024 · Accepted: 15 April 2025 ·

Published Online: 1 May 2025














View Online



Export Citation



CrossMark

Andrew A. Schmidt,^{1,2}  Li-Mor David,^{1,2} Nida T. Qayyum,^{1,2,3}  Khanh Tran,^{1,2}  Cassandra Van,^{4,5,6} 
Ali H. S. H. A. Hetta,^{1,2}  Ronit L. Shrestha,^{1,2} Ashley O. Varatip,^{1,2}  Sergei Butenko,^{1,2}
Daniela Enriquez-Ochoa,^{1,2}  Christy Nguyen,^{4,5}  Marcus M. Seldin,^{4,5}  Wendy F. Liu,^{1,2,3,7,8} 
and Anna Grosberg^{1,2,3,9,a)} 

AFFILIATIONS

¹Department of Biomedical Engineering, University of California, Irvine, Irvine, California 92697, USA

²UCI Edwards Lifesciences Foundation Cardiovascular Innovation and Research Center (CIRC), University of California, Irvine, Irvine, California 92697, USA

³Department of Chemical & Biomolecular Engineering, University of California, Irvine, Irvine, California 92617, USA

⁴Department of Biological Chemistry, University of California, Irvine, Irvine, California 92697, USA

⁵Center for Epigenetics and Metabolism, University of California, Irvine, Irvine, California 92617, USA

⁶Center for Complex Biological Systems, University of California, Irvine, Irvine, California 92697, USA

⁷Department of Molecular Biology and Biochemistry, University of California, Irvine, Irvine, California 92697, USA

⁸Institute for Immunology, University of California, Irvine, Irvine, California 92697, USA

⁹The NSF-Simons Center for Multiscale Cell Fate Research and Sue and Bill Gross Stem Cell Research Center and Center for Complex Biological Systems, University of California, Irvine, Irvine, California 92697, USA

^{a)} Author to whom correspondence should be addressed: grosberg@uci.edu

ABSTRACT

Cardiac adaptation to hypoxic injury is regulated by dynamic interactions between cardiomyocytes and macrophages, yet the impacts of immune phenotypes on cardiac structure and contractility remain poorly understood. To address this, we developed the immuno-heart on a chip, a novel *in vitro* platform to investigate cardiomyocyte-macrophage interactions under normoxic and hypoxic conditions. By integrating neonatal rat ventricular myocytes (NRVMs) and bone marrow-derived macrophages—polarized to pro-inflammatory (M1) or pro-healing (M2/M2*) phenotypes—we elucidated the dual protective and detrimental roles macrophages play in modulating cardiomyocyte cytoskeletal architecture and contractility. Pro-inflammatory stimulation reduced cardiomyocyte structural metrics (z-line length, fraction, and integrity) in normoxic co-cultures. Under hypoxia, M1-stimulated NRVM monocultures exhibited declines in cytoskeletal organization—quantified by actin and z-line orientational order parameters. Relative to monocultures, M1-stimulated co-cultures attenuated hypoxia-induced active stress declines but produced weaker normoxic stresses. In contrast, pro-healing stimulation improved normoxic z-line metrics and preserved post-hypoxia cytoskeletal organization but reduced normoxic contractility. Notably, M2-stimulated macrophages restored normoxic contractility and preserved post-hypoxia systolic stress, albeit with increased diastolic stress. RNAseq analysis of M2-stimulated co-cultures identified upregulated structural and immune pathways driving these hypoxia-induced changes. Cytokine profiles revealed stimulation-specific and density-dependent tumor necrosis factor-alpha and interleukin-10 secretion patterns. Together, these findings quantitatively link clinically relevant macrophage phenotypes and cytokines to distinct changes in cardiac structure and contractility, offering mechanistic insights into immune modulation of hypoxia-induced dysfunction. Moreover, the immuno-heart on a chip represents an innovative framework to guide the development of future therapies that integrate immune and cardiac targets to enhance patient outcomes.

© 2025 Author(s). All article content, except where otherwise noted, is licensed under a Creative Commons Attribution-NonCommercial 4.0 International (CC BY-NC) license (<https://creativecommons.org/licenses/by-nc/4.0/>). <https://doi.org/10.1063/5.0253888>

I. INTRODUCTION

Cardiac hypoxia, a condition characterized by insufficient oxygen supply to the heart, poses a significant threat to cardiac tissue health and function. Hypoxia and its sequelae affect cardiac performance at multiple integrative levels, altering the metabolism and structure of individual cardiomyocytes, contractility across cardiac tissues, and remodeling of the heart as a whole.^{1–7} Although the direct cellular consequences of hypoxia have been previously studied, the complex interplay between cardiomyocytes and the immune system during hypoxia-induced injury remains less clear. In the heart, the cardio-immune response to hypoxic injury is a dynamic process composed of multiple phases: an initial acute inflammatory response, followed by inflammation resolution, and eventual tissue repair.^{6,8} Macrophages of various phenotypes play multi-functional roles across these stages, from clearing apoptotic cells and debris during the acute phase to promoting angiogenesis and matrix remodeling during tissue repair.^{8,9} Recruitment of macrophages, as well as shifts in their phenotypes—from pro-inflammatory (M1) to pro-healing (M2)—are driven by the release of various cytokines, chemokines, and other signaling molecules from damaged tissue, and they are essential for proper orchestration of the entire repair process.^{6–8} However, the innate repair process often leads to suboptimal tissue healing; thus, a better understanding of cell–cell interactions under normal and hypoxic conditions may hold key insights into potential therapeutic interventions to mitigate adverse remodeling and/or facilitate advantageous remodeling. However, the mechanisms that drive cardiomyocyte–macrophage interactions remain largely unexplored due to the challenges of such investigations *in vivo*.

Cardiac tissue function, particularly contractility, is inherently tied to the structural organization and architecture of the cytoskeleton, though this relationship is complex.^{10,11} Under normoxic conditions, the cardiomyocyte cytoskeleton supports robust contraction and relaxation. However, hypoxia disrupts cytoskeletal integrity through disrupted oxygen-sensing pathways, inflammation, and modulation of cytoskeletal mechanical properties.^{3,12,13} Contractility is further exacerbated by hypoxia-induced dysregulation of intracellular calcium handling and cytokine signaling.^{4,13} During early hypoxia, pro-inflammatory cytokines such as tumor necrosis factor- α (TNF- α), interleukin-1 beta (IL-1 β), and interleukin-6 (IL-6), released by both immune and non-immune cells, amplify inflammatory cascades and oxidative stress, leading to sarcomeric breakdown and impaired contractility.^{6,8,14–16} Over prolonged hypoxia or ischemic injury, late-stage signaling, including transforming growth factor beta (TGF- β), further promotes maladaptive remodeling via extracellular matrix (ECM) deposition and fibrosis.^{6,13,16} Despite this understanding of individual pathways, how these processes converge to integrate structural remodeling, immune signaling, and contractile dysfunction remains incomplete, underscoring the need for further investigation of how hypoxia reshapes both immediate and long-term cardiac performance.

Current *in vitro* models often study cardiomyocyte and macrophage responses to hypoxia in isolation, limiting our understanding of the complex, reciprocal interactions that occur when these cell types are co-cultured. While individual responses to hypoxia have been previously characterized, they do not fully capture the emergent properties and cell–cell dynamics present *in vivo*.^{17,18} More recent platforms that have explored cardiomyocyte–macrophage interactions have done so through gene expression, electrophysiology, and calcium handling, yet

most have not considered contractility or quantified structural changes.^{19–21} Among those that did assess contractility, the focus was limited to non-stimulated macrophage co-cultures, without consideration of hypoxic conditions or polarized immune environments.¹⁹ While these studies have provided valuable insights, there remains a lack of comprehensive analysis that creates a significant barrier to advancing our understanding of cardiac pathophysiology and developing targeted therapies for ischemic heart disease.

To address this gap, we have developed the immuno-heart on a chip, an innovative *in vitro* platform designed both to mimic physiologically relevant cardiomyocyte interactions and to elucidate their role in modulating cardiac structure and function under normoxic and hypoxic conditions. By integrating specific macrophage phenotypes, cytokine environments, and co-culture densities, this system enables improved investigations into how immune cells influence cardiomyocyte cytoskeletal architecture and contractility while also capturing the reciprocal impact of cardiomyocytes on macrophage function. Using this platform, we demonstrate that macrophage density and phenotype drive distinct changes in cardiomyocyte structural organization and contractile responses, with hypoxia further modulating these effects. RNA sequencing of M2-stimulated cultures revealed that M2 macrophage presence uniquely upregulates pathways in response to hypoxia not observed in cardiomyocyte monocultures. By simultaneously recapitulating and dissecting the cardio-immune interactions observed *in vivo*, this study not only presents a novel platform to interrogate the mechanisms driving cardiac remodeling and dysfunction in ischemic environments but also contributes insights to the growing body of research exploring therapeutic strategies that target cardiomyocyte–macrophage interactions to preserve cardiac function and improve patient outcomes.^{7,22}

II. RESULTS

A. Pro-inflammatory and pro-healing stimulations and macrophages differentially impact cardiac tissue cytoskeletal architecture

To establish an *in vitro* platform to explore the effect of the immune system on the myocardium, we first exposed Sprague-Dawley neonatal rat ventricular myocyte (NRVM) monocultures to cytokine stimulations associated with various immune activation states (Table III; Fig. 1, top row). We then further investigated how Sprague-Dawley rat bone marrow-derived macrophages (BMDMs) of different phenotypes, induced by these cytokines, affect NRVM structure in co-cultures [Fig. 1(a), bottom row]. For co-cultures, macrophages were seeded at densities reflecting different physiological states of the heart (Table I). The cytokines in M1 stimulations (IFN- γ + lipopolysaccharide (LPS)) drive macrophages toward a pro-inflammatory phenotype associated with an early post-hypoxia cardiac environment, while the cytokines in M2 (IL-4 + IL-13) and M2* (IL-4 + IL-13 + LPS) stimulations induce pro-healing phenotypes characteristic of the late-stage recovery phase following hypoxic injury. A schematic of the immuno-heart on a chip is provided in supplementary material Fig. S2. M2* stimulations model the mixed activation state of inflammatory and reparative cues macrophages encounter *in vivo*, a condition that has been shown to potentiate enhanced wound healing compared to M2 stimulation alone.^{23,24} Note that while the denotation of macrophages into three discrete polarization states—M1, M2, or M2*—is useful *in vitro*, it oversimplifies the heterogeneous nature of macrophage polarization *in vivo*, where plasticity and

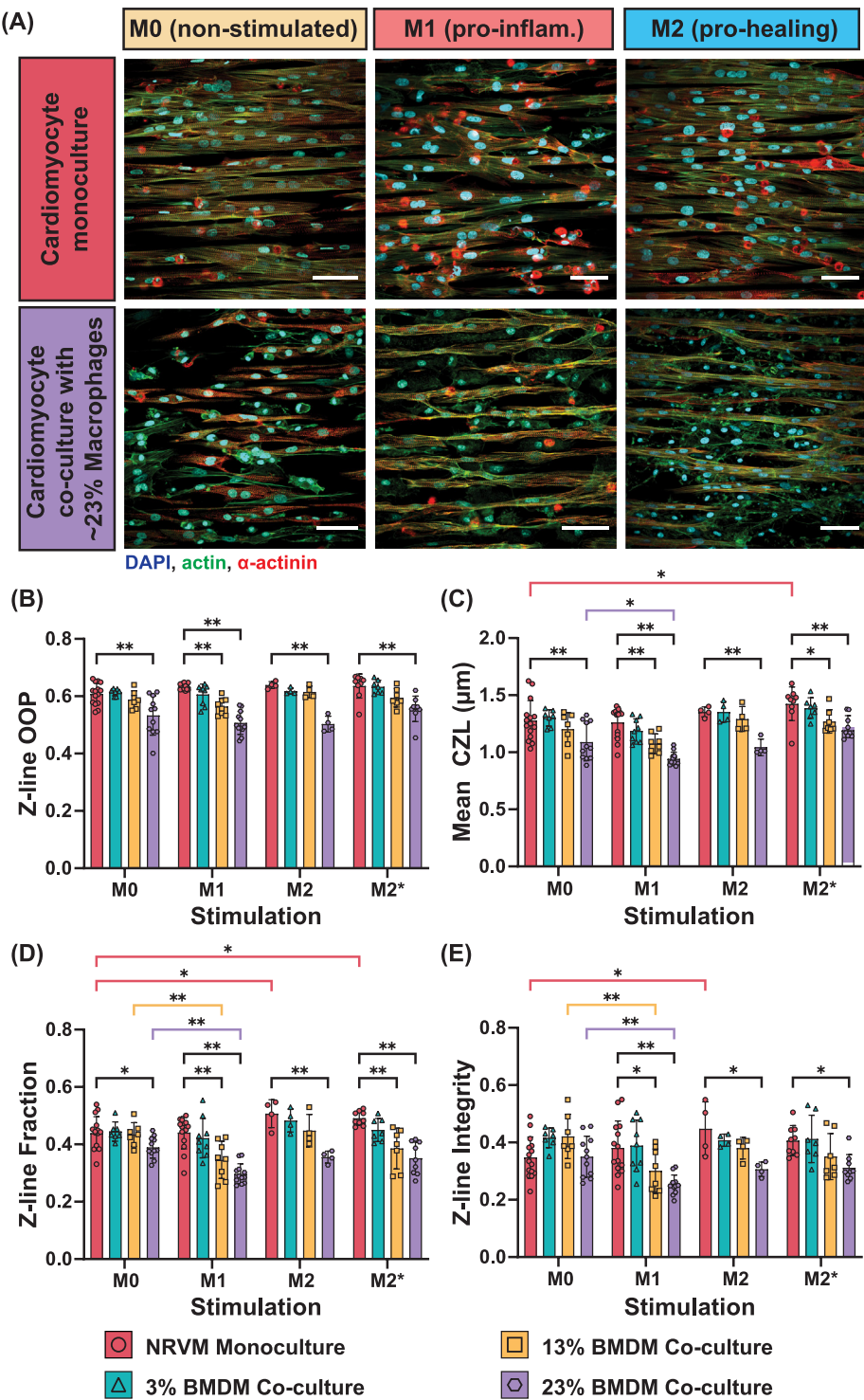


FIG. 1. Cardiac tissue cytoskeletal architecture under various stimulations and macrophage densities. (a) Representative images of NRVM monocultures and NRVM–BMDM juxtacrine co-cultures with the highest experimental density of macrophages (23%) after 24 h of media stimulation [scale bar = 50 μ m; stained for nuclei (blue), actin (green), and α -actinin (red)]. The effect of macrophage seeding density and media stimulation on (b) z-line OOP, (c) mean continuous z-line length, (d) z-line fraction, and (e) z-line integrity (n = 4–15 coverslips; 2–8 harvests per group). Statistical significance was determined by two-way ANOVA with Dunnett’s *post hoc* multiple comparison tests. (Within each stimulation: comparisons to monoculture. Between stimulations and M0 control; colored significance bars: comparison between same BMDM densities.) * p < 0.05, ** p < 0.01.

overlapping phenotypic traits blur rigid categorizations.^{25–28} Nevertheless, for clarity of presentation, the terms M1, M2, and M2* will be used to refer to both the polarized macrophages and the defined cytokine stimulations used to induce each macrophage phenotype

(Table III in Methods). To isolate the effect of cytokines on cardiomyocytes, unstimulated (M0) controls were used as a baseline for comparison. Cardiomyocyte cytoskeletal architecture was quantified using previously developed metrics.^{29,30}

TABLE I. Seeding densities of cardiomyocytes and macrophages for all experiments. Seeding densities of macrophages in co-cultures with cardiomyocytes were selected based on macrophage presence in the heart at different physiological states, ranging from low levels in a healthy heart to increased macrophage densities associated with early- and late-stage post-hypoxic injury.^{8,9}

Seeding density (cells/mm ²)			
Cardiomyocyte	Macrophage	Macrophages/total cells (% ^a)	Physiological equivalent
2.7 × 10 ³	0	0	Cardiomyocyte monoculture
2.7 × 10 ³	8.1 × 10 ¹	~3	Homeostasis
2.7 × 10 ³	4.05 × 10 ²	~13	Late post-hypoxia
2.7 × 10 ³	8.1 × 10 ²	~23	Early post-hypoxia

^aActual percentages at the start of experiments may differ slightly from seeding due to not all cardiomyocytes or macrophages surviving culture.

A BMDM seeding density-dependent reduction in z-line orientational order parameter (OOP) was observed, particularly at early and late post-hypoxia macrophage densities, indicating increased z-line disorganization with higher macrophage presence [Fig. 1(b)]. Similarly, mean continuous z-line length (CZL) decreased with increasing macrophage densities, suggesting a decline in z-line formation and registration (i.e., alignment of z-lines across adjacent sarcomeres in a muscle fiber) or shrinkage of existing z-lines [Fig. 1(c)]. However, M2* media stimulation alone, without the presence of macrophages, significantly increased mean CZL, which may indicate improved z-line development and registration between neighboring myofibrils and cells [Fig. 1(c)]. Since z-line length is calculated from images along the z-disk's edge, higher CZL may also indicate thicker myofibrils. In addition, the z-line fraction, which indicates the fraction of total α -actinin in well-formed z-lines, was significantly reduced in co-cultures with early and late post-hypoxia macrophage densities, suggesting less tissue maturity compared to NRVM monocultures [Fig. 1(d)]. This reduction in maturity was most pronounced under M1 stimulation. In contrast, cytokines in M2 and M2* stimulations of NRVM monocultures seemed to improve z-line maturation, where small, but statistically significant, increases in z-line fraction were observed compared to unstimulated controls [Fig. 1(d)].

To analyze z-line degradation, we developed the z-line integrity (ZLI) fraction metric, which captures the extent of z-line breakdown and diffuse α -actinin presence. The ZLI fraction decreased significantly with higher macrophage densities under M1, M2, and M2* stimulations, indicating increased amounts of diffuse α -actinin signal [Fig. 1(e)]. Notably, unstimulated macrophages, at healthy and late post-hypoxia densities, promoted increased ZLI, suggesting they may exert a stabilizing effect on cardiomyocyte structure in the absence of cytokine stimuli. Further, M2-stimulated media, even in the absence of macrophages, significantly improved ZLI relative to unstimulated media [Fig. 1(e)]. Cytokines associated with M2 media stimulation alone are therefore sufficient to enhance cardiomyocyte z-line stability. These findings indicate that macrophage density and cytokine stimulation influence cardiomyocyte cytoskeletal organization, with some structural parameters affected by stimulation alone, others requiring macrophage presence, and some responding to their combined effects. Importantly, the degree of alterations in z-line OOP, z-line fraction, mean CZL, and ZLI fraction were all significantly dependent [Table II, two-way analysis of variance (ANOVA)] on either the type of macrophage stimulation, seeding density, or their interaction, underscoring

the biological significance of macrophage presence and phenotype in influencing cardiomyocyte structural organization.

B. Cell crowding and paracrine studies

To differentiate between the effects of physical crowding and macrophage-specific influences on cardiomyocyte structure, control experiments were conducted using irradiated mouse embryonic fibroblasts (iMEFs), which served as inert cells occupying space without contributing biologically active signals. These experiments allowed us to distinguish any macrophage-specific effects beyond the impact of cell density. Similar to co-cultures with macrophages, we found that the addition of iMEFs led to decreases in all metrics compared to NRVM monocultures [Figs. 2(a)–2(d)]. However, the magnitude of these effects for z-line OOP, z-line fraction, and z-line integrity fraction differed depending on the seeding density and the added cell type, suggesting that these variations may be influenced both by differences in size between BMDMs and iMEFs and by the distinct biological impact of macrophages compared to the relatively inert nature of irradiated fibroblasts [Figs. 2(a), 2(c), and 2(d)]. Interestingly, the macrophage-induced increase in ZLI was not observed in co-cultures with the fibroblasts [Fig. 2(d)]. Nonetheless, these findings emphasize that at densities above 3%, crowding by another cell type can impact cardiac tissue structure, and any investigation into macrophage effects on cardiac structure or function must include an M0 control to account for these differences.

To study whether paracrine signals might be involved in macrophage phenotype-specific effects on cardiomyocytes, we seeded

TABLE II. Results for two-way ANOVA cytoskeletal response to media stimulation and seeding densities. P-values (p) of significant effects of media stimulations and/or seeding densities and interaction between them are in bold ($p < 0.05$).

Metric	Media		Seeding density		Media × seeding density	
	F	p	F	p	F	p
Z-line OOP	0.8	0.64	4	0.0079	50	<0.0001
Mean CZL	0.8	0.61	17	<0.0001	28	<0.0001
Z-line fraction	2	0.018	11	<0.0001	34	<0.0001
ZLI fraction	2	0.015	5	0.0041	12	<0.0001

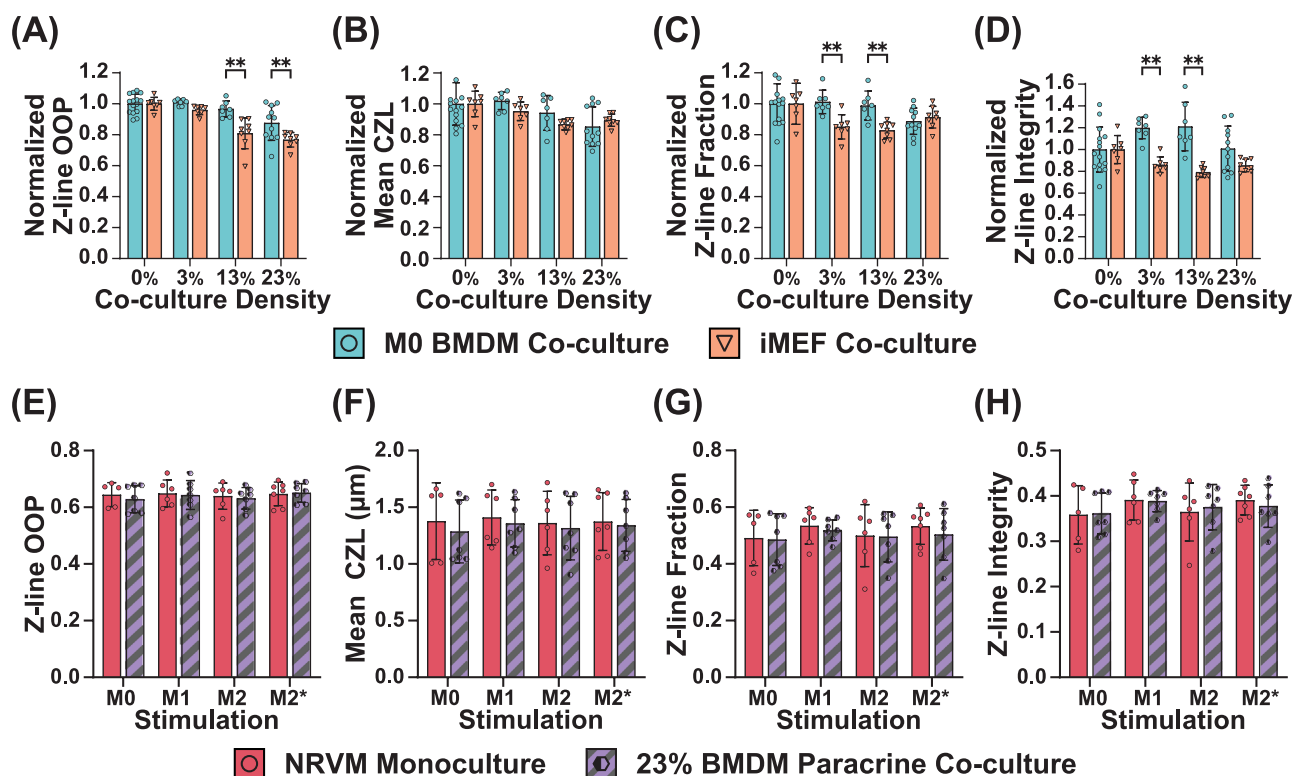


FIG. 2. Comparison of co-culture of NRVMs with irradiated fibroblasts and NRVM-BMDM paracrine co-cultures. (a–d) Comparison of cardiac structural metrics between non-stimulated (M0) co-cultures of NRVMs and BMDMs vs co-cultures of NRVMs and iMEFs. Structural metrics are normalized to 0% monoculture controls associated with each cell type's co-cultures ($n = 7$ –15 coverslips; 3–8 harvests per group). (e–h) Cardiac structural metrics for a paracrine co-culture of NRVMs and BMDMs to determine whether cytokine secretions from stimulated cultures were ample enough to induce NRVM structural changes ($n = 5$ –7 coverslips; 2–3 harvests per group). Statistical significance was determined by two-way ANOVA with Sidak's *post hoc* multiple comparison tests. [(a)–(d) Within each density: comparisons between cell types. (e)–(h) Within each stimulation: comparisons between densities.] ** $p < 0.01$.

NRVMs and BMDMs separately on individual coverslips and then cultured them together within a shared well to allow communication via soluble factors without direct cellular contact. In all media stimulation conditions, there were no significant differences in z-line metrics between NRVM monocultures and NRVM-BMDM paracrine co-cultures at the highest macrophage density [Figs. 2(e)–2(h)]. The changes in z-line metrics observed in juxtacrine experiments were therefore contingent upon contact-mediated signaling between the two cell types, rather than paracrine communication.

C. Differential effects of macrophages on cardiac stress outputs under normoxia

To evaluate how macrophage co-culture impacts cardiac contractility, we fabricated muscular thin film (MTF) contractility assays seeded with NRVM monocultures or NRVM-BMDM co-cultures. The MTFs were electrically paced at 2 Hz to induce contraction, causing the films to curl upwards away from the coverslip and allowing measurement of systolic and diastolic stresses [Fig. 3(a)]. Based on our previous findings on macrophage-influenced changes to cardiomyocyte cytoskeletal architecture, immuno-heart chips of 3% BMDMs

were selected to examine the effect of stimulated macrophages on changes in cardiac contractility.

In monoculture conditions, media stimulation produced significant variability in systolic and diastolic stress, where M2-stimulated cardiomyocytes generated the lowest systolic and diastolic stresses compared to M0, M1, and M2* conditions [Figs. 3(b) and 3(c)]. Since M2 stimulation did not negatively impact most cardiomyocyte structural metrics in NRVM monocultures [Figs. 1(b)–1(d)] and, in fact, enhanced z-line fraction and ZLI [Figs. 1(d) and 1(e)], our data together suggest that the reduced contractile performance of cardiomyocytes in M2 conditions likely stems from nonstructural changes.

Co-culture with macrophages at a homeostatic heart density (~3% BMDMs) significantly reduced the variability in both systolic and diastolic stress outputs across stimulation conditions compared to NRVM monocultures [Figs. 3(b) and 3(c); $p < 0.05$, F -test]. Moreover, within co-culture MTFs, there were no significant differences between stimulation conditions for all stress outputs. This stabilization effect suggests that, under normoxia, macrophages play a role in normalizing cardiomyocyte contractile output under various pro-inflammatory and pro-healing stimulations, possibly by modulating the cytokine environment. Comparing monocultures to co-cultures, the addition of macrophages reduced both systolic and diastolic stress under M0 and

(A) Cardiac Muscular Thin Films

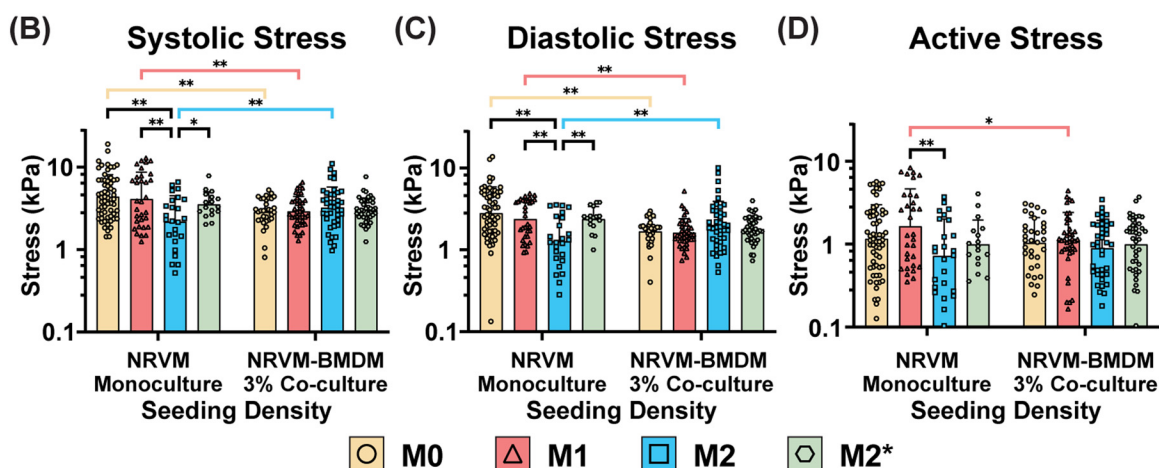
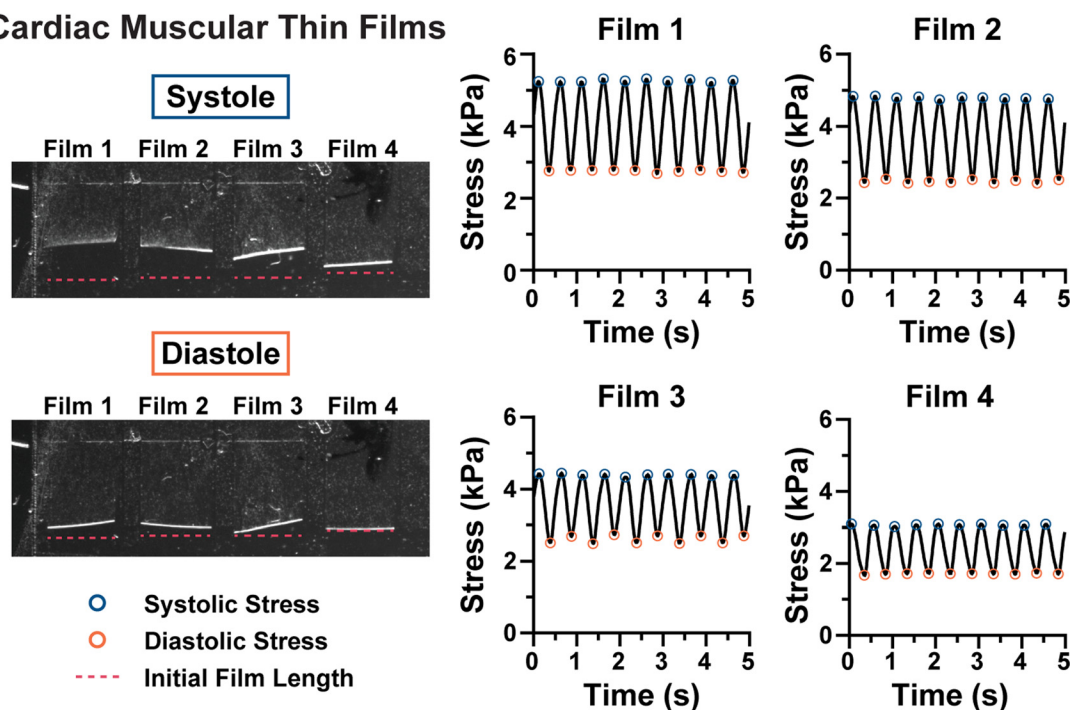


FIG. 3. Effect of media stimulation and macrophage presence on cardiac contractility. (a) Image of muscular thin film assay used to calculate stress and sample traces of stress generated by cardiac tissues of non-stimulated NRVM monocultures. (b) Systolic, (c) diastolic, and (d) active stresses generated by cardiac tissues under varying conditions ($n = 17\text{--}61$ films; 2–7 harvests per group). Statistical significance was determined by two-way ANOVA with Sidak's *post hoc* multiple comparison tests. (Within each density: comparisons between media stimulations. Between each density; colored significance bars: comparison between same media stimulations.) * $p < 0.05$, ** $p < 0.01$.

M1 conditions compared to their respective monoculture controls [Figs. 3(b) and 3(c); yellow and red significance bars]. This reduction may indicate that the presence of macrophages, particularly in M0 and M1 stimulations, inhibits proper stress generation.

In contrast, M2-stimulated co-cultures exhibited a marked improvement in contractile function compared to M2-stimulated cardiac monocultures, bringing their systolic stress on par with the other media stimulations [Fig. 3(b); blue significance bars]. Since this increase in peak stress output by M2-stimulated co-cultures was

paired with a concurrent increase in diastolic stress, the presence of M2 macrophages, or the cytokines they release in their M2 phenotype, may also temper the relaxation ability of cardiac tissues [Fig. 3(c); blue significance bars]. Thus, M2 macrophages provide certain functional advantages in co-culture, while the cytokines driving this phenotype may instead prioritize tissue repair and anti-inflammatory responses over maximizing contractile performance in NRVM monocultures. In terms of active stress, M1-stimulated cultures were alone in seeing a significant difference between

monoculture and co-cultures [Fig. 3(d)]. Indeed, pro-inflammatory cytokines secreted by M1-stimulated macrophages (e.g., TNF- α and IL-6), along with their direct interactions with cardiomyocytes in their inflammatory state, are known to detrimentally impact cardiac contraction.¹⁶ These results demonstrate that macrophage co-culture stabilizes cardiomyocyte contractility across various stimulation conditions and modulates both systolic and diastolic stress in a phenotype-dependent manner.

D. Hypoxia induces reduced NRVM structural metrics, and pro-healing stimulations attenuate hypoxia-induced decreases in cytoskeletal organization

To investigate the combined effects of hypoxia, macrophage density, and cytokine stimulation, the immuno-heart on a chip was subjected to 24 h of 1% O₂. Hypoxia resulted in a qualitative breakdown and disorganization of z-lines and actin filaments [Fig. 4(a)]. In addition to z-line metrics, images of NRVM monocultures were also

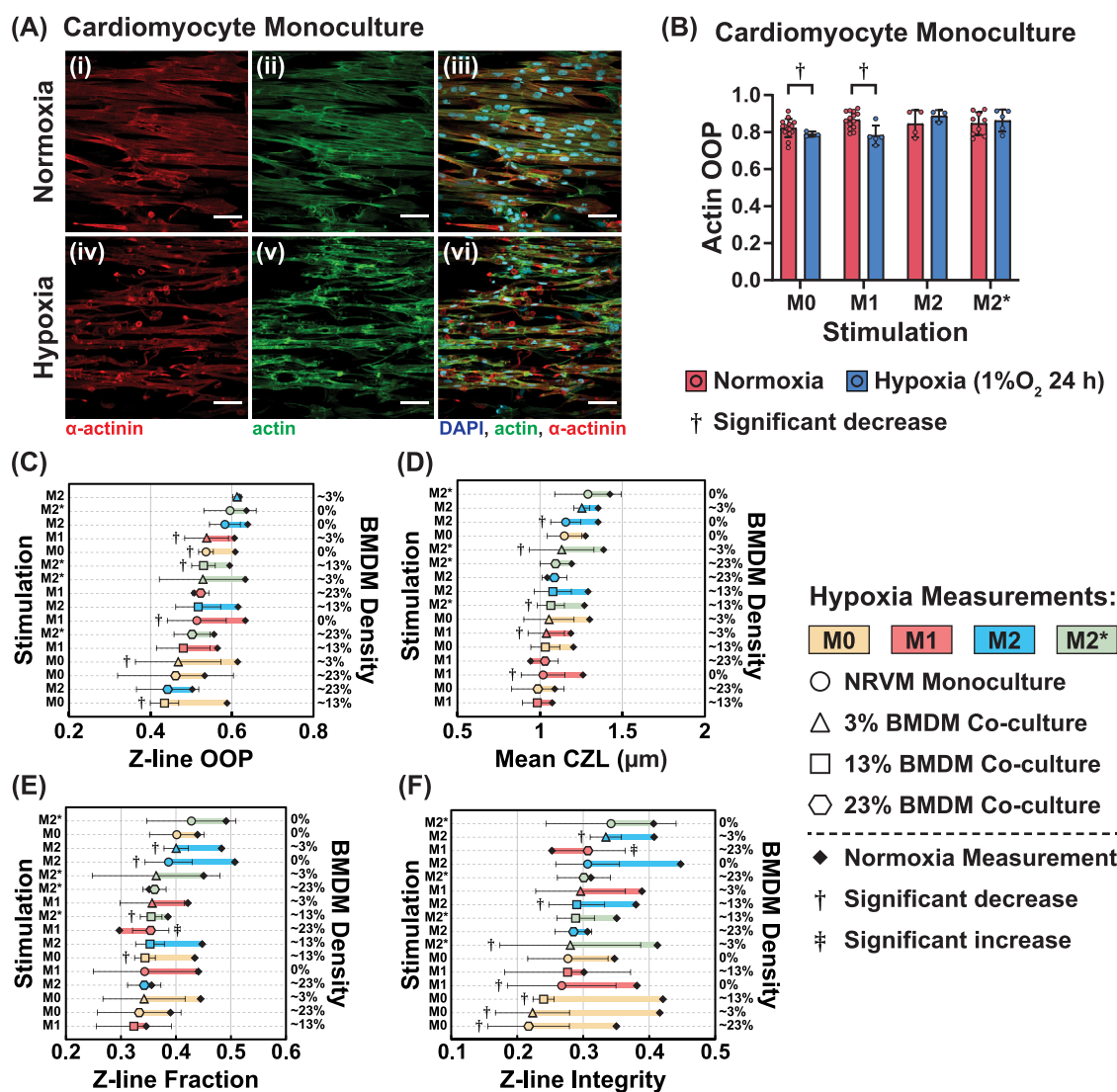


FIG. 4. Cardiomyocyte cytoskeletal changes under hypoxia, stimulatory conditions, and macrophage co-culture. (a) Representative images of non-stimulated NRVM monoculture (Ai–Aiii) normoxic controls and (Aiv–Avi) after 24 h of 1% O₂ hypoxia. (Ai, Aiv) Z-line and (Aii, Av) actin channels show distinct qualitative breakdown and disorganization after hypoxic stimulation relative to normoxic controls. (b) M2- and M2*-stimulated NRVM monocultures attenuate hypoxia-induced reductions in actin cytoskeletal organization metric: actin OOP ($n = 3–15$ coverslips; 2–8 harvests per group). The effect of media stimulations and macrophage seeding density on post-hypoxia: (c) z-line OOP, (d) mean continuous z-line length, (e) z-line fraction, and (f) z-line integrity fraction ($n = 3–5$ coverslips; 1–2 harvests per group). The connected dot plots include normoxia values (Fig. 1, plotted as black diamonds) to illustrate the direction and magnitude of change for each condition. Data are sorted by post-hypoxia values for each metric. Individual sample values for hypoxia measurements are included in [supplementary material](#) Fig. S4. † indicates a significant decrease ($p < 0.05$) relative to normoxic culture; ‡ indicates a significant increase ($p < 0.05$) relative to normoxic culture. [(b)–(f), daggers] Statistical significance was determined by Student's t -tests. (For each condition: comparisons between normoxia and hypoxia.)

analyzed for an actin organizational metric—actin orientational order parameter—to determine the effect of hypoxia on actin organization. Proper actin organization is essential for efficient contraction, structural integrity, and mechanotransduction within cardiomyocytes. Because co-cultures include BMDMs, which exhibit a diffuse, dynamic actin network [Fig. 1(a), bottom row] rather than the structured, aligned filaments necessary for orientational order quantification, actin OOP analysis was only performed for NRVM monocultures. In NRVM monocultures, both z-line and actin OOP metrics in NRVM monocultures showed significant reductions under non-stimulated and pro-inflammatory conditions [Figs. 4(b) and 4(c); daggers]. In contrast, both pro-healing (M2 and M2*) stimulations protected NRVM monocultures from hypoxia-induced drops in z-line and actin OOP, suggesting that the cytokines that induce these macrophage phenotypes may provide some protection against cardiomyocyte cytoskeletal disorganization in response to hypoxia [Figs. 4(b) and 4(c); daggers]. However, M2 stimulation of NRVM monocultures also showed significant reductions in mean CZL and z-line fraction—both metrics that hypoxia did not significantly reduce in non-stimulated monocultures [Figs. 4(d) and 4(e); daggers]. Together with the previous finding, this may indicate that the protective effects of M2 stimulation cytokines against disorganization are accompanied by tradeoffs in metrics related to tissue maturity, z-line registration, and contractile efficiency, potentially reflecting a hypoxia-induced shift in cellular priorities toward stabilization of cytoskeletal components at the expense of optimal structural quality and functionality. It is important to note that the significant hypoxia-induced reduction in z-line fraction of M2-stimulated NRVM monocultures is, in part, due to their normoxic levels being significantly greater than non-stimulated normoxic controls [Fig. 1(d)]. By contrast, NRVM monocultures stimulated with pro-inflammatory cytokines exhibited significant hypoxia-induced decreases in mean CZL and ZLI, changes that were absent in non-stimulated monocultures [Figs. 4(d) and 4(f); daggers]. These findings imply that the presence of pro-inflammatory cytokines amplifies hypoxia-induced z-line degradation, myofibril shrinkage, and disruption of z-line registration. These findings confirm that hypoxia alone is sufficient to induce substantial cytoskeletal breakdown in cardiomyocytes, with pro-inflammatory stimulation providing no additional protection and instead aggravating of structural damage. Remarkably, M2*-stimulated NRVM monocultures demonstrated robust resistance against hypoxia-induced cytoskeletal damage, where none of the measured structural metrics were significantly reduced following hypoxia [Figs. 4(b)–4(f)].

In NRVM–BMDM co-cultures, M1-, M2-, and M2*-stimulated macrophages did not significantly improve post-hypoxia structural metrics compared to non-stimulated controls seeded at the same density [Figs. 4(c)–4(f)]. Interestingly, the presence of M1 macrophages at the 23% seeding density—the expected macrophage density during the acute inflammatory phase following hypoxic injury—appears to improve z-line fraction relative to its normoxic counterpart [Fig. 4(e), double dagger]. Moreover, in terms of z-line integrity, M1 macrophages protect against hypoxia-induced z-line degradation at 3% and 13% densities [Fig. 4(f), daggers], and at 23%, they not only prevent significant drops but also enhance post-hypoxia ZLI [Fig. 4(f), double dagger]. This contrasts with non-stimulated co-cultures at the same densities, which all exhibited significant reductions in ZLI under hypoxia compared to their respective normoxic controls [Fig. 4(f),

daggers]. However, these interpretations should be considered with caution, as the normoxic z-line fraction and ZLI values for M1 co-cultures were already significantly reduced at 13% and 23% BMDM densities relative to normoxic non-stimulated controls at the same densities [Figs. 1(d) and 1(e); yellow and purple significance bars]. Thus, the presence of M1 macrophages in normoxic co-cultures may already compromise z-line fraction and ZLI at the aforementioned densities to such an extent that hypoxia cannot exacerbate the damage further. Alternatively, the presence of M1 macrophages in hypoxic co-cultures may mitigate hypoxia-induced declines or even improve structural metrics by clearing apoptotic or necrotic cardiomyocytes, thereby reducing structural disarray and minimizing secondary damage to z-lines of adjacent cells. Together, these findings underscore the complex and context-dependent role of stimulatory cytokines and macrophages in modulating cardiomyocyte structural integrity, highlighting the need for further investigation into their dual roles in both attenuation and exacerbation of hypoxia-induced effects.

E. Stimulated macrophages rescue hypoxia-induced contractility reduction in cardiomyocytes

Contractility of cardiomyocytes in immuno-heart chips was measured before and after 6 h of 1% O₂ hypoxia, and the relative changes in systolic stress, diastolic stress, and active stress were analyzed. Because the chips are at both the start and end of the hypoxia regimen, each film effectively acts as its own control. Note that any contractile changes are unlikely to result from cellular remodeling upon the films being released from the chip for 6 h, as the strain the cardiomyocytes undergo during the films' bending is <1%³¹ (6-h normoxia comparison in [supplementary material](#) Fig. S5). To quantify the effects of hypoxia on contractility, we measured the relative drop in stress ($d\text{Stress} = \Delta\sigma/\sigma_{0h} = (\sigma_{6h} - \sigma_{0h})/\sigma_{0h}$) in NRVM monocultures and NRVM–BMDM co-cultures (Fig. 5).

In monocultures, there were significant drops ($d\text{Stress} < 0$) in systolic and active stress relative to pre-hypoxia baselines across all stimulation conditions, indicating impaired contractile performance following hypoxia [Figs. 5(a) and 5(c), daggers]. A significant drop in diastolic stress relative to baseline was also observed in non-stimulated monocultures [Fig. 5(b), dagger]. In contrast, co-culture with stimulated macrophages significantly attenuated the hypoxia-induced declines in systolic, diastolic, and active stress compared to non-stimulated co-cultures [Figs. 5(a)–5(c)]. Specifically, M2-stimulated macrophages displayed a protective effect against hypoxia, where co-cultures maintained systolic stress levels after hypoxia, dropping significantly less compared to their M2 monoculture counterpart [Fig. 5(a); blue significance bar]. However, M2 co-cultures also exhibited a significant increase in diastolic stress relative to the pre-hypoxia baseline, which may reflect impaired relaxation or increased passive stiffness in the tissue following hypoxia [Fig. 5(b), double dagger]. Despite stimulated macrophage-mediated protection against systolic and diastolic stress declines, all conditions—both monoculture and co-culture—showed a significant reduction in active stress after hypoxia [Fig. 5(c), daggers]. Non-stimulated macrophage co-cultures experienced a more pronounced drop in active stress compared to monocultures, with some losing all contractile ability after hypoxic stimulation, whereas M1 and M2 co-cultures exhibited significantly less severe drops in active stress relative to their monoculture counterparts [Fig. 5(c); colored significance bars]. These findings suggest that macrophages in

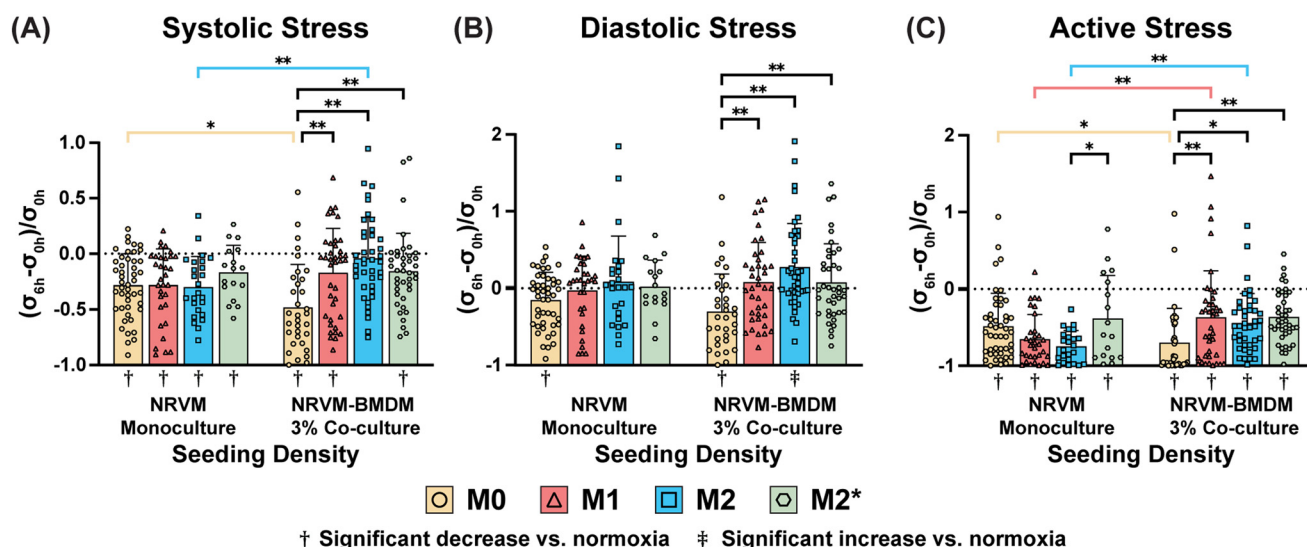


FIG. 5. Hypoxia impacts contractile stress of immuno-heart on a chip. Relative changes in (a) systolic, (b) diastolic, and (c) active stress generated by immuno-heart chips under various media stimulations and co-culture conditions ($n = 17$ –46 films; 2–7 harvests per group). † indicates a significant decrease ($p < 0.05$) in stress relative to the pre-hypoxia baseline; ‡ indicates a significant increase ($p < 0.05$) in stress relative to the pre-hypoxia baseline. [(a)–(c), daggers] Statistical significance was determined by one-sample t -tests or Wilcoxon's signed-rank test. (For each condition: comparisons between normoxia and hypoxia.) [(a)–(c), stars] Statistical significance was determined by two-way ANOVA with Sidak's *post hoc* multiple comparison tests. (Within each density: comparisons between media stimulations. Between each density; colored significance bars: comparison between same media stimulations.) * $p < 0.05$, ** $p < 0.01$.

their stimulated states mitigate the detrimental effects of hypoxia on cardiomyocyte contractile performance, stabilizing diastolic stress (M1 and M2*) while attenuating the loss of active stress (M1, M2, and M2*), with M2 macrophages demonstrating a specific capacity to maintain systolic output but potentially contributing to impaired relaxation dynamics.

F. Co-culture with cardiomyocytes affects macrophage phenotype-specific cytokine secretion

Cardiomyocyte–macrophage communication drives the alternative structural and functional outputs we observe under co-culture conditions; thus, it follows that the various conditions tested also impacted macrophage function reciprocally. This crosstalk impacts both cell types and plays a crucial role in modulating inflammatory responses and maintaining a pro-inflammatory or pro-healing environment.

The immuno-heart on a chip platform was also employed to investigate how cardiomyocyte presence influences macrophage cytokine secretion. ELISA was used to analyze supernatants from M1- and M2*-stimulated cultures. As expected, since M0 and M2 stimulations lack LPS, these macrophage phenotypes remained unactivated and did not secrete cytokines as part of their functional profile (supplementary material Fig. S6).^{32,33} TNF- α levels were measured as a key indicator of a pro-inflammatory environment and M1 macrophage polarization [Figs. 6(a) and 6(b)]. In M1 juxtacrine normoxic co-cultures, where cardiomyocytes and macrophages were in direct physical contact, the presence of NRVMs triggered a significant increase in TNF- α secretion by macrophages, indicating a more active and reinforced M1 phenotype [Fig. 6(a)]. As the entire culture is stimulated by pro-inflammatory cytokines, the cardiomyocytes may also be experiencing

their own inflammatory response. However, cardiomyocyte monocultures were also measured for TNF- α secretion, and the observed levels were minimal to non-detectable [Fig. 6(a)]. The co-culture TNF- α level was, therefore, not the cumulative secretion of the two cell types, suggesting that when macrophages become activated into a pro-inflammatory state, the inflammatory response is further enhanced due to the reciprocal interactions between the cardiomyocytes and macrophages. As a control, TNF- α secretions were also measured in paracrine normoxic co-cultures, where NRVMs and BMDMs shared media but were seeded separately. Under these conditions, co-culture no longer increased TNF- α secretion [Fig. 6(a), striped bar]. Therefore, it is unlikely that M1-stimulated cardiomyocytes are secreting a signaling molecule that furthers M1 macrophage polarization.

This contact-mediated increase in TNF- α secretion by normoxic co-cultures is unique to M1-stimulated cultures, as this increase was not observed in M2* juxtacrine normoxic co-cultures [Fig. 6(b)]. M2* paracrine normoxic co-cultures also did not exhibit different cytokine secretion levels relative to their BMDM monoculture counterparts [Fig. 6(b)]. However, when cultures were subjected to 24 h of 1% O₂ hypoxia, there was a significant increase in TNF- α secretion by M2* juxtacrine co-cultures relative to BMDM monocultures [Fig. 6(b)]. This response indicates that, at the 23% BMDM seeding density, hypoxia amplifies the inflammatory response of TNF- α secretion in M2* co-cultures. Interestingly, hypoxia alone was found to not have any significant effect on TNF- α secretion in cultures of either stimulation.

Cultures were also assayed for their IL-10 secretion, an anti-inflammatory cytokine crucial to the process of cardiac recovery following hypoxic injury and a key indicator of a pronounced pro-healing macrophage phenotype [Figs. 6(c) and 6(d)]. Under M1 stimulation, the presence of cardiomyocytes did not significantly increase

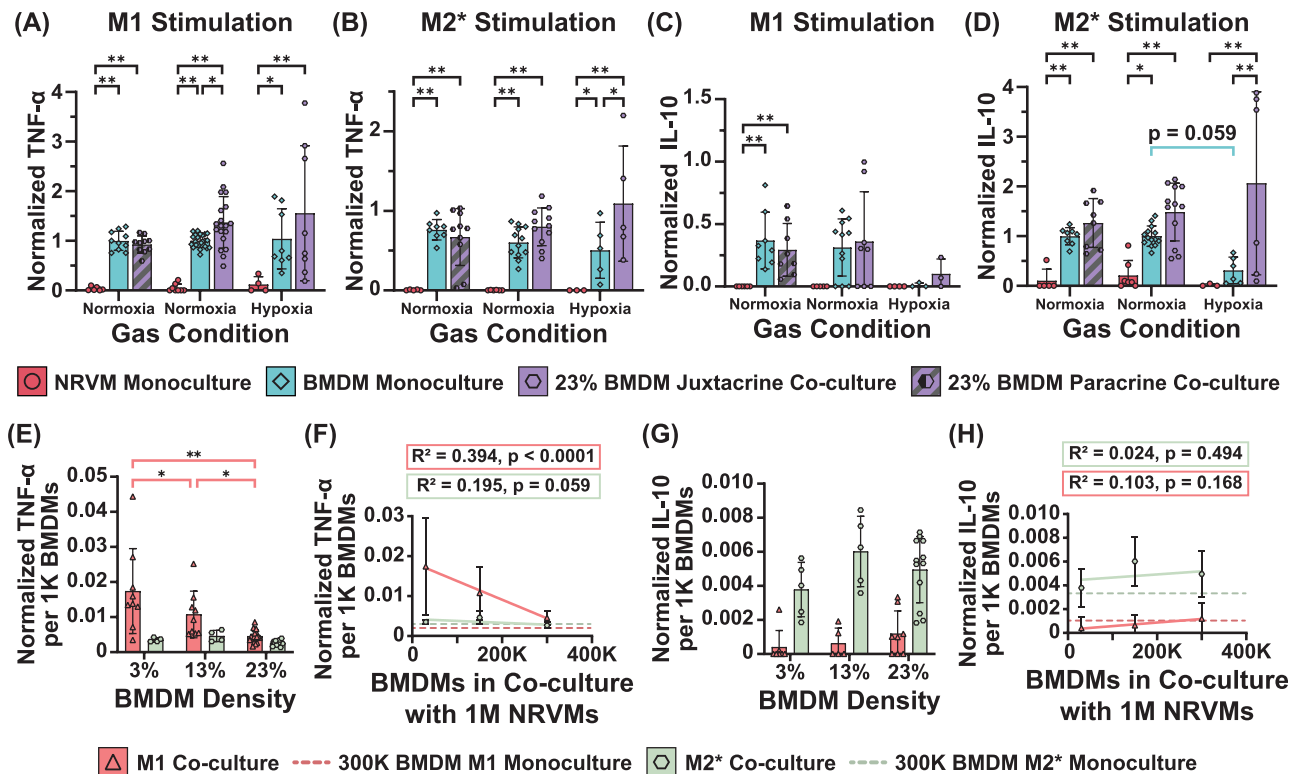


FIG. 6. Cytokine secretion in paracrine normoxic, juxtacrine normoxic, and juxtacrine hypoxic cultures. TNF- α secretion by (a) M1-stimulated cultures and (b) M2*-stimulated cultures. TNF- α secretions are normalized to the average TNF- α levels of normoxic, M1-stimulated macrophage monocultures for each experiment. IL-10 secretion by (c) M1-stimulated cultures and (d) M2*-stimulated cultures. IL-10 secretions are normalized to the average IL-10 levels of normoxic, M2*-stimulated macrophage monocultures for each experiment. Statistical significance was determined by two-way ANOVA with Holm-Sidak's *post hoc* multiple comparison tests. (e)–(h) Cytokine secretion in co-cultures normalized to the number of BMDMs seeded in each culture (per 1 K BMDMs). (f) and (h) Linear regression lines are fit to all data [displayed in (e) and (g)], but only averages are plotted for clarity. Dotted red and green lines indicate TNF- α and IL-10 secretion of 300 K BMDM monocultures (normalized per 1 K BMDMs). (a)–(d) Statistical significance was determined by two-way ANOVA with Holm-Sidak's *post hoc* multiple comparison tests. (Within each gas condition group: comparisons between densities. Between densities; colored significance bars: comparisons between juxtacrine normoxia and juxtacrine hypoxia.) * $p < 0.05$, ** $p < 0.01$. [$N = 4$ –22 coverslips (technical duplicates); 2–10 harvests per group.] (e) and (g) Statistical significance was determined by two-way ANOVA with Tukey's *post hoc* multiple comparison tests. (For each condition: comparisons between BMDM seeding densities.) * $p < 0.05$, ** $p < 0.01$. [$N = 4$ –19 coverslips (technical duplicates); 2–10 harvests per group.] (f) and (h) Linear regression slope determined to be significantly non-zero by a *t*-test. $p < 0.05$.

IL-10 secretion, regardless of culture conditions [Fig. 6(c)]. In M2* normoxic co-cultures, neither juxtacrine nor paracrine interactions with cardiomyocytes significantly increased IL-10 secretion [Fig. 6(d)]. In contrast, IL-10 secretion was significantly increased in M2* hypoxic co-cultures relative to their respective M2* BMDM monoculture controls [Fig. 6(d)], a response in line with the increase in TNF- α secretion by the same cultures [Fig. 6(b)]. This pattern likely reflects that under hypoxic stress, cardiomyocytes produce signals that induce an increased secretion of both inflammatory and anti-inflammatory cytokines by M2* macrophages. Contributing to this finding was the near-significant hypoxia-induced decrease in IL-10 secretion by M2* macrophage monocultures [Fig. 6(d), teal significance bar]. One potential explanation for this decrease is the death of M2* macrophages following the hypoxia regimen, as M2 macrophages rely heavily on aerobic energy production pathways.²⁷

To understand how cardiomyocytes are affecting cytokine secretions at different macrophage seeding densities, TNF- α and IL-10 secretions were normalized to the number of BMDMs in each culture

[Figs. 6(e)–6(h)]. Under pro-inflammatory stimulation, macrophages at lower seeding densities produced greater levels of TNF- α per cell compared to those seeded at higher seeding densities [Figs. 6(e) and 6(g)]. This density dependency, however, was not present in TNF- α secretions by M2*-stimulated co-cultures nor IL-10 secretions by either M1 or M2* co-cultures [Figs. 6(e)–6(h)].

G. Transcriptomic changes in M2-stimulated cultures under hypoxia and normoxia

To gain insight into the transcriptional landscape specifically associated with the M2 pro-healing stimulation and its effects on tissue responses to hypoxia and normoxia, we performed bulk RNAseq analysis of cultures comparing M2-stimulated NRVM monocultures and co-cultures. M2 conditions were selected based on their protective effects on cardiomyocyte cytoskeletal organization and contractility [Figs. 4(b)–4(d) and 5(a)], making them a compelling candidate for transcriptomic analysis. This approach allowed us to examine how M2

stimulation and macrophages influence gene expression changes in response to hypoxia and identify pathways relevant to cardiac adaptation. Samples for sequencing were collected either after 24 h of normoxia or 1% O₂ hypoxia, and for each comparison, all conditions other than gas were held constant in order to isolate the effect of hypoxia. When compared to normoxic NRVM monocultures, pro-healing monocultures responded to hypoxia by significantly downregulating pathways associated with response to lipid, extracellular region, and cytokine/immune responses [Fig. 7(a)]. Attenuation of genes associated with lipid response is consistent with the expected hypoxia-induced metabolic shifts in cardiomyocytes from fatty acid oxidation to anaerobic glycolysis. Deprioritization of fatty acid utilization under hypoxia may also lead to suppression of cellular lipid uptake, transport, and signaling pathways. Hypoxic downregulation of extracellular region pathways in M2-stimulated monocultures may reflect an adaptive response by cardiomyocytes to conserve energy and prioritize essential cellular functions under hypoxic stress, even in the presence of IL-4 and IL-13 stimulation. By minimizing less-critical extracellular interactions—such as extracellular matrix remodeling and paracrine signaling—cardiomyocytes appear to redirect resources toward intracellular stability and metabolic demands. This shift is further supported by the observed downregulation of immune response and cytokine signaling pathways, suggesting a deprioritization of inflammatory and immune-related processes in favor of structural and functional preservation. The suppression of these pathways likely indicates

a reduced reliance on intercellular communication in the absence of immune cells and reflects a cellular focus on maintaining cytoskeletal organization and survival. Together, these findings highlight a coordinated hypoxic adaptation in cardiomyocytes that reduces energy expenditure on non-essential extracellular processes while leveraging pro-healing cytokines to sustain intracellular architecture and ensure survival.

In comparison, M2-stimulated NRVM-BMDM co-cultures (~23% BMDMs) displayed significant upregulation of pathways related to myofibrils, extracellular space, inflammatory responses, defense responses to other organisms, and bacterial responses compared to normoxic M2 co-cultures [Fig. 7(b)]. In terms of cardiac architecture, the upregulation of myofibril-associated pathways suggests enhanced cytoskeletal structure, which is consistent with post-hypoxia findings of mean CZL where M2 and M2* co-cultures show generally greater values [Fig. 4(d), blue and green]. Notably, myofibril pathways were upregulated only in co-cultures, suggesting that M2 macrophages enhance myofibrillar development and organization—an effect absent in hypoxic cardiomyocyte monocultures—which may explain the maintained systolic stress and attenuated active stress reduction observed in M2 co-cultures (Fig. 5).

The upregulation of extracellular space pathways reflects the contributions of both BMDMs and NRVMs. M2 macrophages are known to secrete cytokines such as TGF- β and IL-10 and express matrix metalloproteinases, which directly regulate the extracellular matrix (ECM)

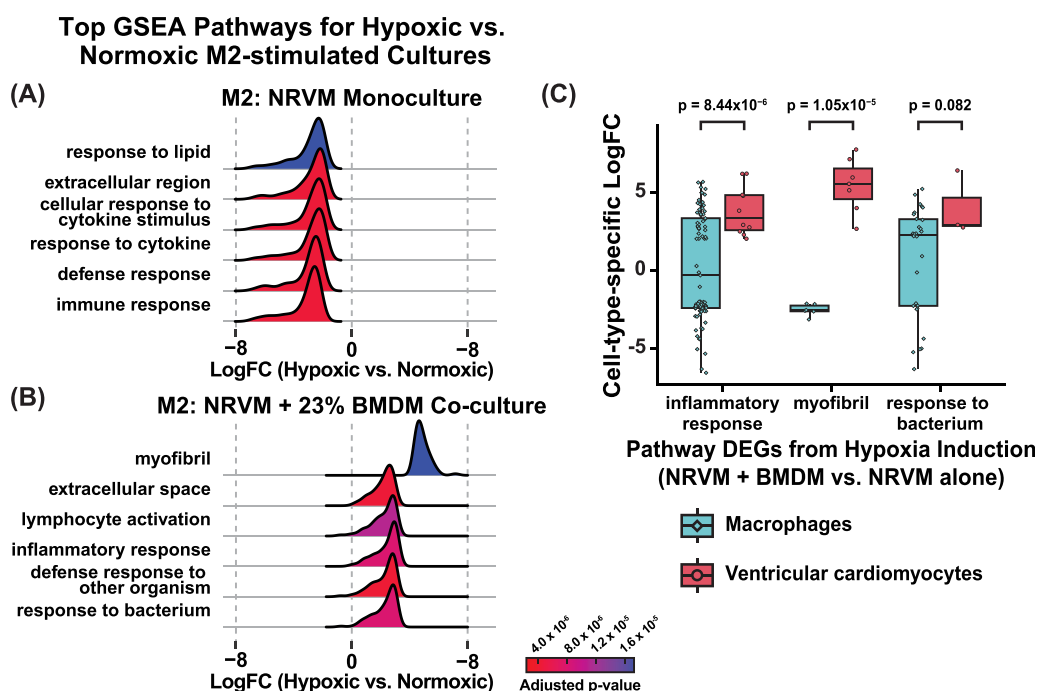


FIG. 7. Bulk RNAseq analysis of hypoxia responses by pro-healing stimulated (M2) co-cultures. Top GSEA pathways (y axis) showing the distribution of log₂-fold changes (x axis) of genes between hypoxic and normoxic M2-stimulated (a) NRVM monocultures and (b) NRVM-BMDM co-cultures (~23% BMDMs). Hypoxia was induced for 24 h at 1% O₂ ($n = 3$ coverslips; 1–2 harvests per group). (c) Boxplots showing the log₂-fold change (y axis) in ventricular cardiomyocytes or macrophages compared to all other cell types in the heart for specific DEGs corresponding to top pathways observed as differently regulated by hypoxia in NRVM-BMDM co-cultures vs NRVM monocultures. Cell-type-specific gene changes are based on the intersection of our bulk RNAseq with previously published single-cell RNAseq data for rat hearts.³⁴ Statistical significance was determined by (a) and (b) GSEA permutation tests comparing weighted logFC for each pathway to the distributions across all genes detected in NRVMs and (c) Wilcoxon *t*-test comparing log₂FC between macrophage and cardiomyocyte expression.

through controlled degradation and collagen stabilization. Cardiomyocytes complement these processes by responding to macrophage-derived signals with ECM-related gene expression. Under hypoxia, macrophage activation by dying cardiomyocytes may further amplify extracellular space-associated pathways. The concurrent upregulation of inflammatory and defense response pathways suggests that hypoxia drives M2 macrophages toward a hybrid phenotype that integrates anti-inflammatory and pro-healing functions with stress-induced immune activation. Notably, M2 macrophages play a recognized role in efferocytosis during cardiac repair, and the hypoxia-induced death of cardiomyocytes (or other macrophages) likely triggers the upregulation of efferocytic gene signaling. This efferocytic activity in BMDMs may account for the observed upregulation of pathways related to defense responses against organisms and bacteria, the latter potentially mediated through macrophage activation by damage-associated molecular patterns (DAMPs) released from necrotic cells. Even within an M2-stimulated environment, macrophages exhibit heightened innate immune activity as an adaptive response to hypoxia, balancing the resolution of hypoxic damage with their reparative roles. These findings highlight the dynamic interplay between cardiomyocytes and macrophages in hypoxic M2 co-cultures, where structural organization, ECM remodeling, and immune activation are integrated into a coordinated and multifaceted adaptive response.

Given that core pathways, such as inflammation, operate in a variety of cell types, we integrated our hypoxia analysis with previously published rat heart single-cell sequencing³⁴ to see which cell-specific genes overlapped with those from hypoxia induction in either NRVMs + BMDMs or NRVMs alone. We note that, despite inflammatory pathways being generally higher in immune cells, the differentially expressed genes (DEGs) analyzed from our hypoxia induction showed higher expression in ventricular cardiomyocytes compared to macrophages. These data show that hypoxia induction on inflammatory pathways acts on core processes such as inflammatory response in both cardiomyocytes and macrophages, supporting the synergistic and unique responses observed in co-culture conditions.

III. DISCUSSION

This study demonstrates that our *in vitro* immuno-heart on a chip platform offers a controlled, adaptable model of cardiac physiology, capable of dissecting the reciprocal interactions between cardiomyocytes and distinct macrophage phenotypes—pro-inflammatory (M1) and pro-healing (M2, M2*)—that influence cardiac tissue structure, contractility, and inflammatory signaling under normoxic and hypoxic conditions. This work contributes an extensive dataset on the *in vitro* interactions of cardiomyocytes and macrophages and the resultant changes in cardiac structure and contractility under normoxic and hypoxic conditions. Together, these demonstrate the power of the developed platform, and further, many of the findings in this work correlate with existing *in vitro* and *in vivo* data.

A. Pro-inflammatory cardiomyocyte-macrophage interactions influence cytoskeletal disruption and TNF- α secretion

For example, under normoxic conditions, M1-stimulated macrophages significantly disrupted cardiomyocyte cytoskeletal structure in co-culture, reducing z-line fraction and z-line integrity at densities mimicking early and late stages of myocardial recovery [Figs. 1(d)

and 1(e)]. Importantly, our paracrine studies revealed that structural changes required direct macrophage–cardiomyocyte contact [Figs. 2(e)–2(h)]. Such interactions echo what occurs in myocardial infarction, where M1 macrophages infiltrate the infarct zone, release pro-inflammatory cytokines such as TNF- α and IL-1 β , and trigger local inflammatory cascades that promote extracellular matrix degradation and cellular injury, often exacerbating cardiac remodeling.^{6,25,35} Indeed, the increased TNF- α secretion in M1 co-cultures compared to M1 macrophage monocultures suggests that macrophage–cardiomyocyte interactions amplify inflammatory signaling [Fig. 6(a)], leading to exacerbated structural damage as you might see following reperfusion *in vivo*. A key limitation of the existing analysis is that actin OOP could only be assessed in NRVM monocultures, as diffuse BMDM actin networks precluded organization analysis. In the future, further refinements in image processing could isolate NRVM-specific actin staining, enabling co-culture effects on cardiomyocyte actin organization to be evaluated.

Under hypoxic conditions, cardiomyocytes in monoculture exhibited significant declines in structural metrics, including actin OOP, z-line OOP, CZL, and ZLI, relative to normoxic controls (Fig. 4). This aligns with *in vivo* and *in vitro* findings where hypoxia induces cardiomyocyte apoptosis and structural disorganization.^{5,36–38} Interestingly, in hypoxic M1-stimulated cultures, TNF- α levels varied more widely compared to normoxic conditions and also did not experience a hypoxia-induced increase [Fig. 6(a)]. This diverges from the typical *in vivo* stabilization of M1 phenotypes and increased TNF- α characteristic of hypoxic injury.^{39,40} This variability may have resulted from hypoxia-induced macrophage apoptosis or heterogeneous cardiomyocyte apoptotic/necrotic responses. The latter variably compounds macrophage secretion of TNF- α in some cultures while potentially activating macrophages' TNF- α autocrine feedback loops in others, leading to a decline in TNF- α by the time of collection.⁴¹ Because this study only assessed cytokine secretion at one end point (24 h), it lacks the temporal granularity to identify the impact of hypoxia or cardiomyocytes on fluctuations in cytokine secretion over time. This warrants future investigation at multiple stimulation and hypoxia time points.

B. Protective effects of pro-healing cytokines on cardiomyocyte cytoskeletal architecture

Conversely, the M2 pro-healing cytokines IL-4 and IL-13 demonstrated a protective effect on cardiomyocyte structure under both normoxic and hypoxic conditions (Figs. 1 and 3). In normoxia, these cytokines alone improved structural maturation metrics in NRVM monocultures [Figs. 1(d) and 1(e)], and M2* stimulation improved z-line fraction and CZL [Figs. 1(c) and 1(d)]. These findings suggest that IL-4 and IL-13 directly influence cardiomyocyte structural organization, promoting maturation and stability. However, the addition of M2/M2* phenotype macrophages under normoxia did not further improve structural metrics and still exhibited density-dependent declines, possibly due to cell crowding effects overshadowing the stimulation-mediated benefits [Figs. 1(b)–1(e)]. Although we addressed crowding as a potential confounder using irradiated fibroblast controls [Figs. 2(a)–2(d)], future studies should examine co-culture configurations further to minimize potential crowding effects while preserving cell–cell interaction dynamics.

After hypoxia, M2-stimulated NRVM monocultures maintained their structural integrity, suggesting a protective role of M2 cytokines against hypoxia-induced damage [Figs. 4(b), 4(c), and 4(f)]. Moreover, M2*-stimulated monocultures showed no significant declines in structural metrics compared to their normoxic counterparts [Figs. 4(b)–4(f)]. These findings in M2/M2* hypoxic and normoxic NRVM monocultures are supported by reports that IL-13 treatment of adult cardiomyocytes strongly phosphorylates both Akt (pAkt) and Erk (pErk), which have been reported to improve contractility and promote a cellular hypertrophic response.^{42–45} Furthermore, studies with cultured neonatal rat cardiomyocytes showed that both IL-4⁴⁶ and IL-13⁴⁷ may contribute to cardiac regeneration via upregulation of the proliferative signaling pathways. Although evidence of the protective roles of IL-4 and IL-13 is emerging, how the individual pathways could converge to coordinate cardiac regeneration is far from comprehensively understood. Since this platform investigates immediate hypoxic effects, it does not capture cardiomyocyte responses that would be observed during inflammatory resolution or remodeling—phases associated with a rise in IL-4 and IL-13 levels *in vivo*. Despite this limitation, our immediate post-hypoxia data still offer biological insights into acute inflammatory interactions crucial during early hypoxic responses. Moving forward, our platform is equipped to interrogate such interactions both individually and in combination with one another.

C. Pro-healing macrophages in a hypoxic cardiac microenvironment

In hypoxic co-cultures, M2 macrophage presence did not meaningfully impact cardiomyocyte structural metrics [Figs. 4(c)–4(f)]. However, these results should be interpreted with the caveat that M2 macrophages are typically found post-reoxygenation *in vivo*. Since they are more reliant on aerobic energy production than M1 macrophages, their function in hypoxic cultures may not fully recapitulate their natural role in ischemic recovery.^{39,48} Based on both *in vitro* and *in vivo* studies,^{35,46,49,50} optimal cardiac repair requires both an acute inflammatory phase with phagocytic clearance and M2 macrophage-derived IL-10 dampening of inflammation.^{48,51–54} This physiology is captured by our M2* co-cultures, where macrophages showed mixed cytokine secretion under hypoxia, with increased TNF- α and IL-10, suggesting hybrid polarization triggered by hypoxic stress and/or cardiomyocyte apoptosis [Figs. 6(b) and 6(d)]. Indeed, hypoxia^{40,55} and inflammatory signaling from damaged tissue^{23,24,26,28} have been shown to regulate macrophage polarization and their cytokine secretion. The emergence of these findings suggests studies using this platform could further characterize macrophage phenotypes by integrating surface marker analysis via flow cytometry and more thorough cytokine profiling through multiplex ELISA. Additionally, analyzing contractility of paracrine co-cultures could further isolate the influence of macrophage signaling on cardiac stress generation. These approaches will help elucidate how reciprocal cellular mechanisms interact with existing immunomodulatory therapies.^{51,54,56–60}

The RNAseq analysis of hypoxic M2-stimulated co-cultures revealed transcriptional changes that provide insight into cardiomyocyte-macrophage interactions under hypoxic stress (Fig. 7). Upregulation of myofibrils, ECM interaction, and immune response pathways emphasizes the coordinated macrophage-mediated adaptation to hypoxia that integrates structural and

inflammatory remodeling. While bulk RNAseq cannot distinguish cardiomyocyte- and macrophage-specific contributions, we leveraged previously published single-cell RNA sequencing of rat hearts to refine how each cell type drives these adaptive responses.³⁴ Despite these insights, future studies applying single-cell RNA sequencing directly within our platform can provide an even more granular understanding of immune-cardiac interactions.

D. Modulation of cell and tissue function by cardiomyocyte-macrophage interactions

Our immuno-heart on a chip platform demonstrates that under normoxic conditions, co-culturing cardiomyocytes with macrophages at physiological densities reduces variability in systolic, diastolic, and active stresses across cytokine stimulation types (Fig. 3). While M0 and M1 cultures both saw decreases in systolic and diastolic stresses between monocultures and co-cultures, M1 stimulation was the only condition that saw a significant decrease in active stress [Figs. 3(b)–3(d)]. These results align with studies that show pro-inflammatory cytokines, especially those associated with M1 macrophage presence such as TNF- α , can reduce cardiomyocyte contractility, impair intracellular calcium handling, and downregulate contractile protein expression.^{61–63} These findings may also support *in vivo* findings where macrophages in inflammatory contexts help mitigate excessive stress responses, supporting cardiac tissue stability during early inflammatory phases.

The reduced contractile performance observed in M2-stimulated monocultures, despite improved structural organization, could indicate that IL-4 and IL-13 alter cardiomyocyte metabolic activity or electromechanical coupling, affecting contractility without affecting structure.⁴⁶ However, this is contrary to some studies that have shown connections between IL-13 treatment and improved cardiac contractility.^{42–45} Interestingly, M2-stimulated co-cultures improved contractile function compared to M2-stimulated monocultures but presented increased diastolic stress [Fig. 3(c)], suggesting that M2-inducing cytokines may enhance structural support over optimal contractility, a known phenomenon where M2 cytokines favor anti-inflammatory and reparative signaling over contractile efficiency.^{49,64} Following hypoxia, the presence of stimulated macrophages mitigated the detrimental effects of low oxygen on cardiomyocyte contractility, in line with their cardioprotective roles observed *in vivo* during cardiac injury.⁶ M2 macrophages, in particular, preserved systolic stress post-hypoxia, suggesting their involvement in enhancing cardiomyocyte survival and function through anti-inflammatory cytokine secretion like IL-10.^{22,27} Recent work has explored the possibility of mitochondrial transfer between M2 macrophages and cardiomyocytes as a means of cardioprotection.^{25,65,66} However, the associated increase in diastolic stress indicates potential impairment in relaxation dynamics relative to their pre-hypoxia baseline [Fig. 5(b)]. This dual effect reflects *in vivo* scenarios where M2 macrophages promote tissue healing but may also contribute to altered contraction if unregulated. Fascinatingly, heart failure with preserved ejection fraction exhibits a greater amount of profibrotic (as opposed to anti-inflammatory) M2 macrophages, which secrete more profibrotic factors that can impair diastolic relaxation.⁴⁸ Future transcriptomic and ELISA analysis of this unique cardiac phenotype can explore this less-studied pathological phenotype.

In investigating the cytokine-mediated crosstalk between cardiomyocytes and macrophages on the immuno-heart on a chip, permaculture TNF- α secretion was observed to increase linearly as

macrophage seeding density decreased [Figs. 6(e) and 6(g)]. Our findings are corroborated by previous work on the density dependency of cytokine secretion by M1-stimulated BMDM monocultures, which also revealed that lower seeding densities lead to greater amounts of TNF- α secreted per cell.⁶⁷ However, these studies were carried out in monocultures, where macrophages at lower densities were distinctly sparse cultures. It is notable that this density-dependent secretion persists even in confluent co-cultures with an abundance of cardiomyocytes. These results reinforce the idea that the mechanism behind this increase in per-cell TNF- α secretion is not mediated by cell–cell contact but by macrophage–macrophage signaling within cultures. Further, cardiomyocyte presence does not actively hamper this relationship between macrophage density and per-cell secretion activity. For IL-10, there were no observed density-dependent changes in per-cell secretion in M1-stimulated co-cultures [Figs. 6(f) and 6(h)]. This finding is somewhat unexpected in the context of the previous macrophage density study,⁶⁷ where greater seeding densities of M1 macrophage monocultures were associated with increased per-cell IL-10 secretion. Therefore, having cardiomyocytes present may dampen the macrophage–macrophage signaling that induces increased per-cell IL-10 secretion observed in macrophage monocultures.

E. Immunomodulatory therapies

Our findings align with ongoing efforts to therapeutically modulate inflammation after ischemic injury.^{51,52,58} Despite promising results in preclinical and *in vitro* studies, broad anti-inflammatory treatments (glucocorticoids, nonsteroidal anti-inflammatory drug (NSAIDs), and cyclosporine) have largely failed in clinical trials, likely due to the dual role of inflammation in both injury and repair.^{51,52,58} Clinical trials targeting IL-1 β (canakinumab) and IL-6 (tocilizumab) suggest that dampening early inflammation can improve cardiac healing, consistent with our data showing that M1 macrophage–cardiomyocyte interactions exacerbate cytoskeletal disruption and amplify TNF- α secretion.^{56,58,60} Preclinical studies have underscored the therapeutic promise of enhancing anti-inflammatory cytokines (IL-4, IL-13, and IL-10) to resolve inflammation and drive macrophage polarization toward reparative phenotypes, aligning with our findings that IL-4/IL-13 stimulation protected against hypoxia-induced cytoskeletal disorganization and M2 macrophage presence preserved systolic stress. However, the pleiotropic nature of cytokines has complicated clinical translation. New strategies like colchicine therapy and pro-resolving mediators further underscore the paradigm that controlling post-infarction inflammation—by either suppressing its damaging effects or accelerating its resolution—can favorably influence cardiac repair.^{68,69} These parallels highlight the translational potential of our immuno-heart on a chip platform to uncover, evaluate, and refine targeted immunomodulatory strategies. Further, the insights from our study contribute to the ongoing efforts to untangle the complexities of immune-driven cardiac repair.

IV. CONCLUSION

Together, these results highlight the platform's value for replicating *in vivo*-like cardiomyocyte–macrophage interactions and uncovering novel cellular responses, offering an effective *in vitro* model to dissect cellular dynamics central to cardiac repair and pathology. By recreating key aspects of the cardiac microenvironment, including cytokine stimulation and hypoxic stress, we can investigate the specific

contributions of macrophage phenotypes, their secreted factors, and direct cell–cell interactions to cardiomyocyte structure and function. The ability to control and manipulate these variables *in vitro* allows for the exploration of mechanisms that are challenging to isolate *in vivo* due to the intricacy of systemic responses. This platform not only validates known *in vivo* interactions but also uncovers novel aspects of cell–cell communication and phenotypic modulation that could inform therapeutic strategies for cardiac repair and regeneration.

V. METHODS

A. Substrate fabrication for structural studies

Cell culture substrates were fabricated as previously described.^{11,70–72} Briefly, large cover glasses (76 \times 83 mm²; Brain Research Laboratories, Newton, MA) were cleaned by sonication in 95% ethanol for 30 min and air-dried. Coverslips were spin coated with 10:1 polydimethylsiloxane (PDMS; Ellsworth Adhesives, Germantown, WI) at 4000 rpm (2.5 min ramp) and cured for 12 h at 60 °C. The glass was then cut into smaller coverslips (14 \times 12.5 mm²) using diamond glass cutters to fit a 12-well plate. Fibronectin (FN; Sigma-Aldrich, St. Louis, MO) was patterned in 22 μ m lines with 3 μ m gaps via microcontact printing.^{11,71} PDMS stamps were sonicated in ethanol for 15 min and coated with 0.05 mg/ml FN for 1 h. Excess FN was removed from stamps using compressed nitrogen prior to printing the patterns onto coverslips. Coverslips were UVO-treated (8 min; Jelight Company, Irvine, CA) for sterilization and surface functionalization before stamping.^{10,11} The patterned coverslips were stored in phosphate-buffered saline (PBS; Thermo Fisher, Grand Island, NY, Gibco Cat#10010049) until cell seeding. This anisotropic surface patterning results in aligned cardiac tissues, mimicking the properties of *ex vivo* heart sections.^{10,71,73}

B. Immuno-heart on a chip fabrication: substrates for muscular thin films (MTFs)

Heart chips were fabricated for functional studies to measure contractile stress generation by muscular thin films.^{10,11} Strips of protective film were placed on the cleaned large cover glass, spaced apart, leaving regions of glass exposed. A layer of poly(*N*-isopropylacrylamide) (PIPAAm) was then spin coated onto the surface and allowed to cure at room temperature for at least 10 min. The protective films were then peeled away, and the cover glass was once again spin coated with 10:1 PDMS to achieve layers 10–15 μ m thick before being cured for at least 12 h at 60 °C. This resulted in alternating regions of the cover glass coated with only PDMS and both PIPAAm and PDMS. Individual chips (~12.7 \times 13.8 mm²) were laser cut (Trotec Speedy 360, Plymouth, MA) from the large cover glass (laser-to-glass). Four “films” were laser cut (laser-to-PDMS) from the chips (2.5 mm in width, spaced 0.6 mm apart). On the day of analysis, the final cut converted the four films into two opposing rows of four films each. Alternatively, heart chips were also manufactured to have two rows of non-opposing films, each with four films. The laser cutter settings were set to score only the PDMS layer without engraving the glass underneath. The chips were micropatterned as detailed above.

C. Cardiomyocytes harvest and culture

All animals for the study were treated according to the Institutional Animal Care and Use Committee of University of

California, Irvine guidelines (IACUC Protocol No. 2022-054) and the NIH Guide for the Care and Use of Laboratory Animals. All experiments were conducted with neonatal rat ventricular myocytes (NRVMs). Ventricular myocardium was extracted from 2-day-old neonatal Sprague-Dawley rats (Charles River Laboratories, Wilmington, MA) as previously described.⁷⁴ Briefly, following resection, the ventricular tissue was washed with Hanks' balanced salt solution buffer (HBSS; Thermo Fisher, Grand Island, NY, Gibco Cat#14170161) and incubated overnight on a rocker (12 h) at 4 °C in 1 mg/ml trypsin solution (Sigma-Aldrich, St. Louis, MO) dissolved in HBSS. The trypsin was then neutralized with 37 °C M199 culture media (Thermo Fisher, Grand Island, NY, Gibco Cat#11150067) supplemented with 10% fetal bovine serum (FBS; Thermo Fisher, Grand Island, NY, Gibco Cat#26140079). Then, the tissue was washed four times with 1 mg/ml collagenase type II (Worthington Biochemical Corporation, Lakewood, NJ) dissolved in HBSS. The cell solutions were centrifuged at 1000 rpm for 7 min, resuspended in chilled HBSS, and once again centrifuged at 1000 rpm for 7 min. The cells were resuspended in warm 10% FBS M199 culture media and plated onto three consecutive pre-plates to isolate the cardiomyocytes via the different adhesion rates of cardiomyocytes and fibroblasts. The final purified cardiomyocyte solution was seeded onto the FN-coated coverslips or heart chips at 2.7×10^3 cells/mm² in 12-well plates. Cells were supplemented with additional FBS until a final concentration of 30% FBS M199 culture media was achieved. After 24 h post-seeding, the media was replaced with fresh 30% FBS M199 culture media. Forty-eight hours after initial seeding, the dead cells were washed away with PBS, and the remaining cells were incubated in 10% FBS M199 culture media. Contractile and structural studies were performed 4 days after seeding.

D. MTF analysis of contractile stress by cardiac tissues

On the day of contractility studies, heart chips were cut with a razor parallel to the PIPAAm lines, releasing the films and allowing them to contract vertically away from the chip. Any waste portions of PDMS or extraneous films were peeled away manually using forceps. The contractility experiments were performed by placing the heart chips into 35 mm Petri dishes filled with the relevant culture media. The Petri dish was placed onto a temperature-controlled heating plate under a stereo microscope (Olympus America, Center Valley, PA). A mounted camera (Basler, Germany) recorded the film's movements from the top of the microscope at 100 fps. The tissues were field stimulated by a pulsatile field stimulator (Myopacer, IonOptix, Westwood, MA) via two carbon electrodes (McMaster-Carr, Douglasville, GA) spaced 1.5 cm apart. The contractile behavior of the films was

measured as the films were paced at 2 Hz with a voltage of 20 V. Stress measurements were calculated from recorded videos of the films using automated ImageJ and MATLAB codes through the calculations described in Ref. 10.

E. Macrophage harvest and culture

All macrophage experiments were conducted with rat bone marrow-derived macrophages (BMDMs). Femur bones from adult Sprague-Dawley female rats (Charles River) were harvested and flushed with rat D10 media for bone marrow extraction. Flushed bone marrow was treated with ACK Lysing Buffer (Thermo Fisher) before centrifugation and resuspension for lysing of red blood cells leaving white blood cells intact. White blood cells were then seeded on standardized non-treated polystyrene Petri dishes in rat D10 media. Cells were fed for 3–4 days after harvesting. With the essence of macrophage colony-stimulating factor (M-CSF), seeded white blood cells/monocytes were differentiated into BMDMs ready for use 6–8 days after harvesting. As BMDMs are sticky cells, seeding and freezing down require the usage of a cell dissociation buffer (Thermo Fisher) for lifting. Upon lifting, BMDMs were either seeded for experiments or frozen down to be stored in a liquid nitrogen tank at a density of 5×10^6 cells/ml.

F. Cardiomyocyte-macrophage co-culture and stimulation

Juxtacrine co-culture of cardiomyocytes and macrophages was achieved by seeding both cell types onto a single coverslip. NRVMs were harvested and seeded as described above. Forty-eight hours post-seeding of NRVMs, coverslips were rinsed with PBS to wash away any dead NRVMs, and non-stimulated (M0) macrophages were seeded at the required densities in M0 media: a co-culture common media composed of 10% FBS M199 culture media supplemented with 100 U/ml penicillin, 100 μg/ml streptomycin (Thermo Fisher, Grand Island, NY), 2 mM L-glutamine, and 20 ng/ml carrier-free recombinant rat M-CSF (BioLegend, San Diego, CA). Media stimulation and polarization of the macrophages were performed 24 h after the M0 macrophages were seeded in the co-culture. To stimulate the cultures, a quarter of the M0 media in each well was replaced with cytokine-stimulated media (M1, M2, or M2*; Table III). Twenty-four hours after stimulation, supernatants were gathered for ELISA, and coverslips were fixed and stained for structural analysis. Hypoxia regimens for structural and cytokine studies were started concurrently with media stimulation of co-cultures. Hypoxia regimens for contractility studies were shorter than those of structural studies (6 vs 24 h, respectively); therefore, hypoxia for contractility studies was started 24 h after media stimulation to

TABLE III. Media stimulations and components.

Media stimulation	Components	Full components
M199	M199	Medium 199, Earle's salts + glucose + B12 + L-glutamine + FBS + penicillin + streptomycin + HEPES + MEM NEAAs
M0	M199 + M-CSF	M199 + M-CSF
M1	M0 + IFN-γ + LPS	M199 + M-CSF + IFN-γ + LPS
M2	M0 + IL-4 + IL-13	M199 + M-CSF + IL-4 + IL-13
M2*	M2 + LPS	M199 + M-CSF + IL-4 + IL-13 + LPS

ensure macrophages had ample time to differentiate into the proper phenotype prior to hypoxic stimulation. For structural control studies of NRVM co-cultures with irradiated mouse embryonic fibroblasts (iMEFs; Thermo Fisher, Grand Island, NY), iMEFs were seeded with M199 media onto coverslips 48 h after seeding NRVMs.

To achieve **M1** macrophage polarization, a cytokine-stimulated media composed of M0 media with 10 ng/ml of *E. coli*-derived LPS (Sigma-Aldrich, St. Louis, MO) and 10 ng/ml of *E. coli*-derived carrier-free recombinant rat IFN- γ (BioLegend, San Diego, CA) was used. M0 media with 20 ng/ml of 293E-derived carrier-free recombinant rat IL-4 (BioLegend, San Diego, CA) and 20 ng/ml of *E. coli*-derived carrier-free recombinant rat IL-13 (BioLegend, San Diego, CA) was used to stimulate BMDMs into one branch of the M2 phenotype: **M2**. The addition of 10 ng/ml of *E. coli*-derived LPS to IL-4 and IL-13 cytokine-stimulated media creates another branch of M2 phenotype: LPS-activated M2 (**M2**^{*}).

Previous work confirms that the selected concentrations are adequate for proper stimulation, and ELISA provided a functional assessment of macrophage polarization, measuring TNF- α and IL-10, which are well-established indicators of M1 and M2^{*} activation, respectively.^{75–77} Prior studies have shown that cytokine secretion correlates with classical macrophage surface markers used in flow cytometry for polarization assessment.^{23,55} Finally, LPS-induced cytotoxicity in NRVMs was not a major concern at the chosen concentration, as neonatal cardiomyocytes possess innate protective mechanisms that mitigate LPS-induced apoptosis.^{78,79} Nonetheless, to account for potential viability effects, α -actinin and actin confluency were analyzed across all conditions. The results confirmed that neither LPS nor hypoxia compromised viability to an extent that would invalidate our structural and functional metrics (supplementary material Fig. S7).

G. Cardiomyocyte-macrophage paracrine co-culture

Paracrine co-culture of cardiomyocytes and macrophages was achieved by seeding each cell type onto its own coverslip. Both coverslips were micropatterned with fibronectin anisotropic lines. Cardiomyocytes were prepared the same as in juxtacrine co-cultures. Twenty-four hours after cardiomyocytes were seeded onto their coverslips, unstimulated macrophages were seeded in M0 media onto their own coverslips in a separate 12-well plate. After 24 h, one coverslip of each cell type was moved into a 6-well plate such that they were not in direct contact with each other. The co-culture was replenished with fresh M0 media. The next day, a quarter of the media in each well was replaced with the relevant stimulation media (Table III). After 24 h of stimulation, supernatants were collected for ELISA, and coverslips were fixed and stained for structural analysis.

H. Inducing sustained hypoxia

The experimental setup for hypoxia experiments utilized a temperature-controlled hypoxia chamber and gas flow controller system (Noxygen, Elzach, Germany). Nitrogen, carbon dioxide, and oxygen flowed from compressed tanks (Airgas, Radnor, PA) into the gas flow controller module via three input lines. The gas flow controller was programmed to adjust the flow rates of each gas in the module's output line, resulting in a 94% N₂, 5% CO₂, 1% O₂ hypoxic gas mixture delivered to the incubation chamber. Validation of the hypoxia chamber was performed by measuring oxygen levels of both the

atmosphere and media inside wells within the chamber using a FOSPOR AI-300 optical oxygen-sensing probe and NeoFox-GT phase fluorimeter (Ocean Insight, Orlando, FL). An initial flushing of the chamber with a 95% N₂, 5% CO₂, 0% O₂ gas mixture was performed to quickly bring the chamber down to 1%O₂. Flow rates were chosen such that oxygen levels within the media reached the desired 1% O₂ within 15–20 min. The hypoxia chamber was maintained at 37°C for all experiments. Four days after initial seeding, the coverslips were transferred from 12-well plates to 35 mm dishes in order to reduce the media head prior to placement within the hypoxia chamber. A water tray filled with MilliQ water was placed at the bottom of the chamber to maintain humidity.

I. Fixing, immunostaining, and image acquisition

After conclusion of stimulation, cells were rinsed with ice-cold PBS three times before being fixed on their coverslips in warm 4% paraformaldehyde (PFA; VWR, Radnor, PA) supplemented with 0.05% Triton X-100 (Sigma-Aldrich, St. Louis, MO) for 10 min. Cells were then rinsed three times with room temperature PBS, allowing the PBS to sit for 5 min between rinses. The cells were then stained for nuclei (4',6-diamidino-2-phenylindole dihydrochloride, DAPI; Invitrogen, Waltham, MA), actin (Alexa Fluor 488 Phalloidin; Thermo Fisher, Grand Island, NY), and sarcomeric α -actinin (Mouse Monoclonal Anti α -actinin; Sigma-Aldrich, St. Louis, MO) by incubating the coverslips in 1:200 dilutions in PBS for 1 h at room temperature. The coverslips were rinsed, and then secondary staining was performed with goat anti-mouse IgG secondary antibodies (Alexa Fluor 594; Thermo Fisher, Grand Island, NY) 1:200 dilutions in PBS for 1 h at room temperature. Coverslips were then mounted onto microscope slides using either ProlongTM Gold antifade mountant or ProlongTM Glass antifade mountant (Invitrogen, Waltham, MA) and kept at 4°C until imaged. Immunofluorescence imaging of coverslips was performed using an Olympus Fluoview FV3000 microscope (Olympus America, Center Valley, PA, USA) with a UPLSAPO 40 \times silicone oil immersion objective (Olympus America, Center Valley, PA, USA). The resolution of the images taken at 40 \times was \sim 6.5 pixels/ μ m. Ten to thirty fields of view were randomly acquired for each sample.

J. Image analysis

Analysis of cardiac tissue images and quantification of cytoskeleton structural and organizational metrics were performed by automated MATLAB codes described previously.^{10,29,80} Binary skeletons of α -actinin, the primary protein of sarcomere z-discs, were extracted from microscopy images and analyzed for z-line orientation order parameter (OOP), z-line length, z-line fraction, and z-line integrity. Images of the actin channel for each culture were similarly processed and analyzed for actin OOP.

Z-line integrity is a cytoskeleton structural metric designed to calculate the degree of z-line degradation and amount of diffuse α -actinin protein within cells. In perfect tissue, α -actinin is present in the z-line construct. However, z-line degradation can cause the α -actinin to be present outside the z-band. Consequently, for such a scenario, the signal for α -actinin staining will be more diffuse compared to that of perfect tissue. The fraction of α -actinin staining on the z-lines was analyzed as a metric of z-line integrity

$$\{Z - \text{line Integrity Fraction}\} = \frac{\tau \cdot S_{\{\text{overlay}\}}}{S_{\{\text{original}\}}} \quad (1)$$

τ is a fitting parameter representing a unitless z-line thickness, which we expect to vary based on microscope resolution ($\tau = 5.68$ for the current analysis), and was determined using cropped images of “perfect” tissue from normoxia controls. A visualization of z-line integrity’s τ determination can be found in [supplementary material](#) Fig. S2. Assuming a z-line integrity of 1 for each cropped field of view, Eq. (1) can be rearranged to calculate individual τ values, that are then averaged to determine the τ used for analysis of all images ($\tau = 5.68$ for the current study)

$$\tau = \frac{S_{\{\text{original}\}}}{S_{\{\text{overlay}\}}}, \quad (2)$$

$$S = \sum_{n=1}^j \sum_{c=1}^h \sum_{x \geq 0, y \geq 0}^{\forall x, \forall y} i_{n,c}(x, y), \quad (3)$$

where n represents a single field-of-view image, j is the total number of fields of view for a single coverslip, c is a single color channel, h is the total number of color channels, and (x, y) are the horizontal and vertical coordinates of a pixel on the image, with $(0,0)$ as the location of the bottom left pixel, and i is the pixel’s intensity value. An overlay of the original α -actinin-stained image, the z-line skeleton, and a background output was used to determine $S_{\{\text{overlay}\}}$ for each field of view. On the other hand, an overlay of only the original α -actinin-stained image and a background output was used to determine $S_{\{\text{original}\}}$. The z-line skeleton and background were output from the ZlineDetection code.²⁹ The background output provides an estimate of pixels not stained for α -actinin and sets them as black, which is useful for microscopes that do not have pseudo-coloring ability. Based on Eq. (1), the theoretical range for z-line integrity is from τ to 0, for the case of α -actinin staining only on the identified z-line pixels and the case of no α -actinin staining on the z-line pixels, respectively. For “perfect” tissue, we expect the z-line integrity to be around 1.

K. RNA sequencing and analysis

After the conclusion of the experiments, RNA was extracted from cultures using Qiagen miRNAeasy columns (Qiagen, Hilden, Germany) according to standard manufacturer protocol. Quality control was then performed on an argument bioanalyzer, where RIN scores over 6 were used for sequencing. Libraries were prepared using NEBNext kits (New England Biolabs, Ipswich, MA) from polyA-isolated mRNA, then pooled at 4M concentration for sequencing. Libraries were sequenced on a NovaSeq 6000 (Illumina, San Diego, CA) using paired-end sequencing at a depth of 20×10^6 reads/sample.

FASTQ files obtained from sequencing were inspected using FastQC and aligned to the rat transcriptome (Rnor 6.0) using Kallisto. Transcript-level counts were then extracted from the Kallisto outputs, averaged at the gene level and differential expression (DE) was performed using DESeq2. Specifically, samples were isolated into comparable categories (e.g., NRMVS alone or NRVM + BMDMs), and DE was performed on hypoxia vs normoxia. Prior to DE, genes that showed an estimated counts less than 10 across samples were removed. Pathway enrichments were performed using gseGO from DESeq2 logFC. Therefore, samples with mixed cell types (BMDM + NRVMs) were only compared to each other, and NRVM monocultures were

compared directly. Lists of DEGs resulting from comparing hypoxia in matched cell types were then compared at the results level in order to ensure proper overlap among comparisons. **Single-cell integration:** To investigate which cells expressed DEGs corresponding to hypoxia induction, cell-specific marker genes were used from Arduini *et al.*³⁴ Specifically, genes that showed cell-specific expression ($p\text{-adj} < 0.01$) in macrophages or ventricular cardiomyocyte cell populations were analyzed. The log2FC for cell-specific differential expression was plotted for DEGs corresponding to specific pathways in the hypoxia vs normoxia NRVM + BMDM comparisons. P-values shown correspond to a Wilcoxon t -test comparing the cell-specific log2FC between macrophage and cardiomyocyte expression (y axis) for indicated DEG pathways (x axis).

L. ELISA

Analysis of cytokine secretion was performed using ELISA kits (BioLegend, San Diego, CA). Prior to fixing or lysing the cells for structural and transcriptomic analysis, 800 μl of media from each culture’s well was placed into an Eppendorf (one Eppendorf per sample). The Eppendorfs were spun down at 2000 rcf for 5 min at 4 °C to settle any debris. Then, 400 μl of the supernatant from each Eppendorf was moved into 2 wells (200 μl per well; technical duplicates) of a low-adhesion 96-well plate. Samples were frozen at -20°C until ELISA was performed. The supernatants were analyzed for the presence of TNF- α and IL-10 according to the kit’s manufacturer’s instructions. For each experiment, values of TNF- α and IL-10 were normalized to those of M1 and M2* BMDM monocultures, respectively.

M. Statistical analysis

GraphPad Prism version 10 was used to conduct all statistical tests. To determine statistical significance in studies with two factors, a two-way analysis of variance (ANOVA) was performed, with Tukey’s, Sidak’s, and Dunnett’s *post hoc* tests for multiple comparisons when appropriate. A two-way ANOVA with a Holm–Sidak’s multiple comparison test was used for ELISA data when comparing datasets with distinctly near-zero control values. To determine whether stress outputs significantly changed from baseline in contractility experiments, one-sample t -tests were conducted against a constant that would indicate no change in stress (i.e., 0) if normality of the data were assumed. Otherwise, a one-sample Wilcoxon signed-rank test was performed. To determine a significant difference for a factor with only two levels (e.g., normoxia vs hypoxia) independent from other experimental conditions, Student’s t -tests were performed between the two levels. Following two-way ANOVA, a p -value of less than 0.05 was considered significant. Outliers were initially identified using the ROUT method ($Q = 0.1\%$) and were subsequently evaluated within the experimental context. Outliers were removed if there was a clear indication of experimental error or if they represented values significantly outside the distribution range defined by the majority of the data. Data are presented as mean \pm standard deviation. All the data were compiled into a database as described previously⁸¹ and in the [supplementary material](#).

SUPPLEMENTARY MATERIAL

See the [supplementary material](#) for a schematic of the immuno-heart on a chip, visualization of the z-line integrity cytoskeleton structural metric, raw values of z-line metrics for NRVM–iMEF

co-cultures, individual sample values for post-hypoxia z-line metrics for all conditions, 6-h normoxia contractility control data, additional cytokine secretion values for M0- and M2-stimulated cultures, and analysis of α -actinin and actin confluency.

ACKNOWLEDGMENTS

We are thankful to Dr. Rami Khayat, Benjoseph Villanova, Jonovan Osario, Ashley Niu, and Hui Eng Lim for their contributions to the development of this work. This work was partially supported by NIH T32HL116270 (A. S.), DoD NDSEG Fellowship (A. S.), NSF CMMI-2035264 (A. G.), NSF CMMI-2230503 (A. G.), and NIH R03 EB028605 (A. G.).

AUTHOR DECLARATIONS

Conflict of Interest

The authors have no conflicts to disclose.

Ethics Approval

Ethics approval for experiments reported in the submitted manuscript on animal or human subjects was granted. NRVM and BMDM samples were acquired in accordance with the Institutional Animal Care and Use Committee of University of California, Irvine guidelines (IACUC Protocol No. 2022-054) and the NIH Guide for the Care and Use of Laboratory Animals.

Author Contributions

Andrew A. Schmidt: Conceptualization (equal); Data curation (equal); Formal analysis (equal); Funding acquisition (equal); Investigation (equal); Methodology (equal); Project administration (equal); Software (equal); Validation (equal); Visualization (equal); Writing – original draft (equal); Writing – review & editing (equal). **Li-Mor David:** Conceptualization (equal); Formal analysis (equal); Investigation (equal); Methodology (supporting); Project administration (equal). **Nida Qayyum:** Data curation (equal); Software (equal); Writing – review & editing (equal). **Khanh Tran:** Data curation (equal); Formal analysis (equal); Investigation (supporting); Writing – review & editing (equal). **Cassandra Van:** Data curation (supporting); Investigation (supporting); Software (supporting). **Ali H. S. H. A. Hetta:** Investigation (supporting); Validation (equal). **Ronit L. Shrestha:** Formal analysis (supporting); Investigation (supporting); Validation (equal). **Ashley O. Varatip:** Formal analysis (supporting); Investigation (supporting); Validation (equal). **Sergei Butenko:** Formal analysis (equal); Investigation (supporting). **Daniela Enriquez-Ochoa:** Investigation (supporting). **Christy Nguyen:** Data curation (supporting); Investigation (supporting). **Marcus Seldin:** Data curation (supporting); Formal analysis (supporting); Funding acquisition (supporting); Project administration (equal); Resources (supporting); Supervision (supporting); Writing – review & editing (supporting). **Wendy F. Liu:** Conceptualization (equal); Funding acquisition (equal); Project administration (equal); Resources (equal); Supervision (equal); Writing – review & editing (equal). **Anna Grosberg:** Conceptualization (equal); Funding acquisition (equal); Project administration (equal); Resources (equal); Software (equal); Supervision (equal); Writing – original draft (equal); Writing – review & editing (equal).

DATA AVAILABILITY

The data that support the findings of this study are openly available through Dryad at <https://doi.org/10.5061/dryad.0k6djhbc7>, Ref. 82.

REFERENCES

- 1S. Frantz, M. J. Hundertmark, J. Schulz-Menger, F. M. Bengel, and J. Bauersachs, “Left ventricular remodelling post-myocardial infarction: Pathophysiology, imaging, and novel therapies,” *Eur. Heart J.* **43**(27), 2549–2561 (2022).
- 2P. M. Kang, A. Haunstetter, H. Aoki, A. Usheva, and S. Izumo, “Morphological and molecular characterization of adult cardiomyocyte apoptosis during hypoxia and reoxygenation,” *Circ. Res.* **87**(2), 118–125 (2000).
- 3S. F. Steinberg, “Oxidative stress and sarcomeric proteins,” *Circ. Res.* **112**(2), 393–405 (2013).
- 4R. Wang, M. Wang, S. He, G. Sun, and X. Sun, “Targeting calcium homeostasis in myocardial ischemia/reperfusion injury: An overview of regulatory mechanisms and therapeutic reagents,” *Front. Pharmacol.* **11**, 872 (2020).
- 5A. Elias-Llumbet, R. Sharmin, K. Berg-Sorensen, R. Schirhagl, and A. Mzyk, “The interplay between mechanoregulation and ROS in heart physiology, disease, and regeneration,” *Adv. Healthcare Mater.* **13**(23), 2400952 (2024).
- 6N. G. Frangogiannis, “The inflammatory response in myocardial injury, repair and remodeling,” *Nat. Rev. Cardiol.* **11**(5), 255–265 (2014).
- 7J. Yap, J. Irei, J. Lozano-Gerona, S. Vanapruks, T. Bishop, and W. A. Boisvert, “Macrophages in cardiac remodelling after myocardial infarction,” *Nat. Rev. Cardiol.* **20**(6), 373–385 (2023).
- 8Y. Kim, S. Nurakhayev, A. Nurkesh, Z. Zharkinkbekov, and A. Saparov, “Macrophage polarization in cardiac tissue repair following myocardial infarction,” *Int. J. Mol. Sci.* **22**(5), 2715 (2021).
- 9M. Nahrendorf, F. K. Swirski, E. Aikawa, L. Stangenberg, T. Wurdinger, J.-L. Figueiredo, P. Libby, R. Weissleder, and M. J. Pittet, “The healing myocardium sequentially mobilizes two monocyte subsets with divergent and complementary functions,” *J. Exp. Med.* **204**(12), 3037–3047 (2007).
- 10A. Grosberg, P. W. Alford, M. L. McCain, and K. K. Parker, “Ensembles of engineered cardiac tissues for physiological and pharmacological study: Heart on a chip,” *Lab Chip* **11**(24), 4165–4173 (2011).
- 11M. B. Knight, N. K. Drew, L. A. McCarthy, and A. Grosberg, “Emergent global contractile force in cardiac tissues,” *Biophys. J.* **110**(7), 1615–1624 (2016).
- 12P. Razezghi, M. F. Essop, J. M. Huss, S. Abbasi, N. Manga, and H. Taegtmeier, “Hypoxia-induced switches of myosin heavy chain iso-gene expression in rat heart,” *Biochem. Biophys. Res. Commun.* **303**(4), 1024–1027 (2003).
- 13J. Veldhuizen, R. Chavan, B. Moghadas, J. G. Park, V. D. Kodibagkar, R. Q. Migrino, and M. Nikkha, “Cardiac ischemia on-a-chip to investigate cellular and molecular response of myocardial tissue under hypoxia,” *Biomaterials* **281**, 121336 (2022).
- 14M. Buoncervello, S. Maccari, B. Ascione, L. Gambardella, M. Marconi, M. Spada, D. Macchia, T. Stati, M. Patrizio, W. Malorni, P. Matarrese, G. Marano, and L. Gabriele, “Inflammatory cytokines associated with cancer growth induce mitochondria and cytoskeleton alterations in cardiomyocytes,” *J. Cell. Physiol.* **234**(11), 20453–20468 (2019).
- 15J. E. Van Eyk, F. Powers, W. Law, C. Larue, R. S. Hodges, and R. J. Solaro, “Breakdown and release of myofilament proteins during ischemia and ischemia/reperfusion in rat hearts,” *Circ. Res.* **82**(2), 261–271 (1998).
- 16Y. Jian, X. Zhou, W. Shan, C. Chen, W. Ge, J. Cui, W. Yi, and Y. Sun, “Crosstalk between macrophages and cardiac cells after myocardial infarction,” *Cell Commun. Signal.* **21**(1), 109 (2023).
- 17E. Riboldi, C. Porta, S. Morlacchi, A. Viola, A. Mantovani, and A. Sica, “Hypoxia-mediated regulation of macrophage functions in pathophysiology,” *Int. Immunol.* **25**(2), 67–75 (2013).
- 18M. L. Rexius-Hall, N. N. Khalil, S. S. Escopete, X. Li, J. Hu, H. Yuan, S. J. Parker, and M. L. McCain, “A myocardial infarct border-zone-on-a-chip demonstrates distinct regulation of cardiac tissue function by an oxygen gradient,” *Sci. Adv.* **8**(49), eabn7097 (2022).
- 19R. I. Lock, P. L. Graney, D. N. Tavakol, T. R. Nash, Y. Kim, E. Sanchez, M. Morsink, D. Ning, C. Chen, S. Fleischer, I. Baldassarri, and G. Vunjak-Novakovic, “Macrophages enhance contractile force in iPSC-derived human engineered cardiac tissue,” *Cell Rep.* **43**(6), 114302 (2024).

- ²⁰T. Hutschalik, O. Özgül, M. Casini, B. Szabó, R. Peyronnet, Ó. Bártulos, M. Argenziano, U. Schotten, and E. Matsa, "Immune response caused by M1 macrophages elicits atrial fibrillation-like phenotypes in coculture model with isogenic hiPSC-derived cardiomyocytes," *Stem Cell Res. Ther.* **15**(1), 280 (2024).
- ²¹P. G. Hitscherich, L.-H. Xie, D. Del Re, and E. J. Lee, "The effects of macrophages on cardiomyocyte calcium-handling function using in vitro culture models," *Physiol. Rep.* **7**(13), e14137 (2019).
- ²²Z. Zhang, J. Tang, X. Cui, B. Qin, J. Zhang, L. Zhang, H. Zhang, G. Liu, W. Wang, and J. Zhang, "New insights and novel therapeutic potentials for macrophages in myocardial infarction," *Inflammation* **44**(5), 1696–1712 (2021).
- ²³T. D. Smith, M. J. Tse, E. L. Read, and W. F. Liu, "Regulation of macrophage polarization and plasticity by complex activation signals," *Integr. Biol.* **8**(9), 946–955 (2016).
- ²⁴E. M. O'Brien and K. L. Spiller, "Pro-inflammatory polarization primes macrophages to transition into a distinct M2-like phenotype in response to IL-4," *J. Leukocyte Biol.* **111**(5), 989–1000 (2022).
- ²⁵R. Chen, H. Zhang, B. Tang, Y. Luo, Y. Yang, X. Zhong, S. Chen, X. Xu, S. Huang, and C. Liu, "Macrophages in cardiovascular diseases: Molecular mechanisms and therapeutic targets," *Signal Transduction Targeted Ther.* **9**(1), 1–44 (2024).
- ²⁶R. Zaman, H. Hamidzada, and S. Epelman, "Exploring cardiac macrophage heterogeneity in the healthy and diseased myocardium," *Curr. Opin. Immunol.* **68**, 54–63 (2021).
- ²⁷A. Shapouri-Moghaddam, S. Mohammadian, H. Vazini, M. Taghadosi, S.-A. Esmaeili, F. Mardani, B. Seifi, A. Mohammadi, J. T. Afshari, and A. Sahebkar, "Macrophage plasticity, polarization, and function in health and disease," *J. Cell. Physiol.* **233**(9), 6425–6440 (2018).
- ²⁸P. J. Murray, J. E. Allen, S. K. Biswas, E. A. Fisher, D. W. Gilroy, S. Goerdt, S. Gordon, J. A. Hamilton, L. B. Ivashkiv, T. Lawrence, M. Locati, A. Mantovani, F. O. Martinez, J.-L. Mege, D. M. Mosser, G. Natoli, J. P. Saeij, J. L. Schultze, K. A. Shirey, A. Sica, J. Suttles, I. Udalova, J. A. van Ginderachter, S. N. Vogel, and T. A. Wynn, "Macrophage activation and polarization: Nomenclature and experimental guidelines," *Immunity* **41**(1), 14–20 (2014).
- ²⁹T. A. Morris, J. Naik, K. S. Fibben, X. Kong, T. Kiyono, K. Yokomori, and A. Grosberg, "Striated myocyte structural integrity: Automated analysis of sarcomeric z-discs," *PLoS Comput. Biol.* **16**(3), e1007676 (2020).
- ³⁰T. A. Morris, S. Eldeen, R. D. H. Tran, and A. Grosberg, "A comprehensive review of computational and image analysis techniques for quantitative evaluation of striated muscle tissue architecture," *Biophys. Rev.* **3**(4), 041302 (2022).
- ³¹P. W. Alford, A. W. Feinberg, S. P. Sheehy, and K. K. Parker, "Biohybrid thin films for measuring contractility in engineered cardiovascular muscle," *Biomaterials* **31**(13), 3613–3621 (2010).
- ³²J. Y. Hsieh, T. D. Smith, V. S. Meli, T. N. Tran, E. L. Botvinick, and W. F. Liu, "Differential regulation of macrophage inflammatory activation by fibrin and fibrinogen," *Acta Biomater.* **47**, 14–24 (2017).
- ³³H. Atcha, A. Jairaman, J. R. Holt, V. S. Meli, R. R. Nagalla, P. K. Veerasubramanian, K. T. Brumm, H. E. Lim, S. Othy, M. D. Cahalan, M. M. Pathak, and W. F. Liu, "Mechanically activated ion channel Piezo1 modulates macrophage polarization and stiffness sensing," *Nat. Commun.* **12**(1), 3256 (2021).
- ³⁴A. Arduini, S. J. Fleming, L. Xiao, A. W. Hall, A.-D. Akkad, M. D. Chaffin, K. J. Bendinelli, N. R. Tucker, I. Papangeli, H. Mantineo, P. Flores-Bringas, M. Babadi, C. M. Stegmann, G. García-Cardena, M. E. Lindsay, C. Klattenhoff, and P. T. Ellinor, "Transcriptional profile of the rat cardiovascular system at single-cell resolution," *Cell Rep.* **44**(1), 115091 (2025).
- ³⁵Z. Yang, B. Zingarelli, and C. Szabó, "Crucial role of endogenous interleukin-10 production in myocardial ischemia/reperfusion injury," *Circulation* **101**(9), 1019–1026 (2000).
- ³⁶E. Bouhamida, G. Morciano, M. Perrone, A. E. Kahsay, M. Della Sala, M. R. Wiekowski, F. Fiorica, P. Pinton, C. Giorgi, and S. Patergnani, "The interplay of hypoxia signaling on mitochondrial dysfunction and inflammation in cardiovascular diseases and cancer: From molecular mechanisms to therapeutic approaches," *Biology* **11**(2), 300 (2022).
- ³⁷J. P. S. Nunes, P. Andrieux, P. Brochet, R. R. Almeida, E. Kitano, A. K. Honda, L. K. Iwai, D. Andrade-Silva, D. Goudenège, K. D. Alcantara Silva, R. S. Vieira, D. Levy, S. P. Bydlowski, F. Gallardo, M. Torres, E. A. Bocchi, M. Mano, R. H. B. Santos, F. Bacal, P. Pomerantzeff, F. R. M. Laurindo, P. C. Teixeira, H. I. Nakaya, J. Kalil, V. Procaccio, C. Chevillard, and E. Cunha-Neto, "Co-Exposure of cardiomyocytes to IFN- γ and TNF- α induces mitochondrial dysfunction and nitro-oxidative stress: Implications for the pathogenesis of chronic Chagas disease cardiomyopathy," *Front. Immunol.* **12**, 755862 (2021).
- ³⁸Z. Iwoń, E. Krogulec, A. Kierlańczyk, M. Wojasiński, and E. Jastrzębska, "Hypoxia and re-oxygenation effects on human cardiomyocytes cultured on polycaprolactone and polyurethane nanofibrous mats," *J. Biol. Eng.* **18**, 37 (2024).
- ³⁹A. Viola, F. Munari, R. Sánchez-Rodríguez, T. Scolaro, and A. Castegna, "The metabolic signature of macrophage responses," *Front. Immunol.* **10**, 1462 (2019).
- ⁴⁰A. Lewis and P. M. Elks, "Hypoxia induces macrophage tnfa expression via cyclooxygenase and prostaglandin E2 in vivo," *Front. Immunol.* **10**, 2321 (2019).
- ⁴¹J. M. Gane, R. A. Stockley, and E. Sapey, "TNF- α autocrine feedback loops in human monocytes: The pro- and anti-inflammatory roles of the TNF- α receptors support the concept of selective TNFR1 blockade *in vivo*," *J. Immunol. Res.* **2016**, 1079851.
- ⁴²A. B. Nik, S. Alvarez-Argote, and C. C. O'Meara, "Interleukin 4/13 signaling in cardiac regeneration and repair," *Am. J. Physiol. Heart Circ. Physiol.* **323**(5), H833 (2022).
- ⁴³D. J. Wodsedalek, S. J. Paddock, T. C. Wan, J. A. Auchampach, A. Kenarsary, S.-W. Tsaih, M. J. Flister, and C. C. O'Meara, "IL-13 promotes in vivo neonatal cardiomyocyte cell cycle activity and heart regeneration," *Am. J. Physiol. Heart Circ. Physiol.* **316**(1), H24–H34 (2019).
- ⁴⁴I. Shiojima, S. Schiekofe, J. G. Schneider, K. Belisle, K. Sato, M. Andrassy, G. Galasso, and K. Walsh, "Short-term Akt activation in cardiac muscle cells improves contractile function in failing hearts," *Am. J. Pathol.* **181**(6), 1969–1976 (2012).
- ⁴⁵M. Mutlak and I. Kehat, "Extracellular signal-regulated kinases 1/2 as regulators of cardiac hypertrophy," *Front. Pharmacol.* **6**, 149 (2015).
- ⁴⁶C. Zogbi, N. C. Oliveira, D. Levy, S. P. Bydlowski, V. Bassaneze, E. A. Neri, and J. E. Krieger, "Beneficial effects of IL-4 and IL-6 on rat neonatal target cardiac cells," *Sci. Rep.* **10**(1), 12350 (2020).
- ⁴⁷C. C. O'Meara, J. A. Wamstad, R. A. Gladstone, G. M. Fomovsky, V. L. Butty, A. Shrikumar, J. B. Gannon, L. A. Boyer, and R. T. Lee, "Transcriptional reversion of cardiac myocyte fate during mammalian cardiac regeneration," *Circ. Res.* **116**(5), 804–815 (2015).
- ⁴⁸M. Kang, H. Jia, M. Feng, H. Ren, J. Gao, Y. Liu, L. Zhang, and M.-S. Zhou, "Cardiac macrophages in maintaining heart homeostasis and regulating ventricular remodeling of heart diseases," *Front. Immunol.* **15**, 1467089 (2024).
- ⁴⁹P. Krishnamurthy, J. Rajasingh, E. Lambers, G. Qin, D. W. Losordo, and R. Kishore, "IL-10 inhibits inflammation and attenuates left ventricular remodeling after myocardial infarction via activation of STAT3 and suppression of HuR," *Circ. Res.* **104**(2), e9–e18 (2009).
- ⁵⁰M. C. Manukyan, C. H. Alvernaz, J. A. Poynter, Y. Wang, B. D. Brewster, B. R. Weil, A. M. Abarbanell, J. L. Herrmann, B. J. Crowe, A. C. Keck, and D. R. Meldrum, "Interleukin-10 protects the ischemic heart from reperfusion injury via the STAT3 pathway," *Surgery* **150**(2), 231–239 (2011).
- ⁵¹S. Huang and N. G. Frangogiannis, "Anti-inflammatory therapies in myocardial infarction: Failures, hopes and challenges," *Br. J. Pharmacol.* **175**(9), 1377–1400 (2018).
- ⁵²D. Mahtta, D. Sudhakar, S. Koneru, G. V. Silva, M. Alam, S. S. Virani, and H. Jneid, "Targeting inflammation after myocardial infarction," *Curr. Cardiol. Rep.* **22**(10), 110 (2020).
- ⁵³M. Jung, Y. Ma, R. P. Iyer, K. Y. DeLeon-Pennell, A. Yabluchiansky, M. R. Garrett, and M. L. Lindsey, "IL-10 improves cardiac remodeling after myocardial infarction by stimulating M2 macrophage polarization and fibroblast activation," *Basic Res. Cardiol.* **112**(3), 33 (2017).
- ⁵⁴S. K. Verma, P. Krishnamurthy, D. Barefield, N. Singh, R. Gupta, E. Lambers, M. Thal, A. Mackie, E. Hoxha, V. Ramirez, G. Qin, S. Sadayappan, A. K. Ghosh, and R. Kishore, "Interleukin-10 treatment attenuates pressure overload-induced hypertrophic remodeling and improves heart function via signal transducers and activators of transcription 3-dependent inhibition of nuclear factor- κ B," *Circulation* **126**(4), 418–429 (2012).
- ⁵⁵F. Raggi, S. Pelassa, D. Pierobon, F. Penco, M. Gattorno, F. Novelli, A. Eva, L. Varesio, M. Giovarelli, and M. C. Bosco, "Regulation of human macrophage

- M1–M2 polarization balance by hypoxia and the triggering receptor expressed on myeloid cells-1,” *Front. Immunol.* **8**, 1097 (2017).
- ⁵⁶F. He, T. Xie, D. Ni, T. Tang, and X. Cheng, “Efficacy and safety of inhibiting the NLRP3/IL-1 β /IL-6 pathway in patients with ST-elevation myocardial infarction: A meta-analysis,” *Eur. J. Clin. Invest.* **53**(11), e14062 (2023).
- ⁵⁷S. Alvarez-Argote, S. J. Paddock, M. A. Flinn, C. W. Moreno, M. C. Knas, V. A. Almeida, S. L. Buday, A. Bakhshian Nik, M. Patterson, Y.-G. Chen, C.-W. Lin, and C. C. O’Meara, “IL-13 promotes functional recovery after myocardial infarction via direct signaling to macrophages,” *JCI Insight* **9**(2), e172702 (2024).
- ⁵⁸M. Panahi, A. Papanikolaou, A. Torabi, J.-G. Zhang, H. Khan, A. Vazir, M. G. Hasham, J. G. F. Cleland, N. A. Rosenthal, S. E. Harding, and S. Sattler, “Immunomodulatory interventions in myocardial infarction and heart failure: A systematic review of clinical trials and meta-analysis of IL-1 inhibition,” *Cardiovasc. Res.* **114**(11), 1445–1461 (2018).
- ⁵⁹D. Lu, J. Fan, Y. Lin, K. Yang, F. Zheng, T. Ma, and F. Zhu, “IL-4 attenuates myocardial infarction injury by promoting M2 macrophage polarization,” *Ann. Med. Surg.* **86**(6), 3349–3356 (2024).
- ⁶⁰S. Toldo, B. W. Van Tassell, and A. Abbate, “Interleukin-1 blockade in acute myocardial infarction and heart failure,” *J. Am. Coll. Cardiol.* **2**(4), 431–433 (2017).
- ⁶¹M. Patten, E. Krämer, J. Bünnemann, C. Wenck, M. Thoenes, T. Wieland, and C. Long, “Endotoxin and cytokines alter contractile protein expression in cardiac myocytes in vivo,” *Pflügers Archiv* **442**(6), 920–927 (2001).
- ⁶²K. Urschel and I. Cicha, “TNF- α in the cardiovascular system: From physiology to therapy,” *Int. J. Interferon Cytokine Mediator Res.* **7**, 9–25 (2015).
- ⁶³M. Tian, Y.-C. Yuan, J.-Y. Li, M. R. Gionfriddo, and R.-C. Huang, “Tumor necrosis factor- α and its role as a mediator in myocardial infarction: A brief review,” *Chronic Dis. Transl. Med.* **1**(1), 18–26 (2015).
- ⁶⁴S. Dhingra, A. K. Sharma, R. C. Arora, J. Slezak, and P. K. Singal, “IL-10 attenuates TNF- α -induced NF κ B pathway activation and cardiomyocyte apoptosis,” *Cardiovasc. Res.* **82**(1), 59–66 (2009).
- ⁶⁵Y. Liu, M. Wu, C. Zhong, B. Xu, and L. Kang, “M2-like macrophages transplantation protects against the doxorubicin-induced heart failure via mitochondrial transfer,” *Biomater. Res.* **26**(1), 14 (2022).
- ⁶⁶Y. Pang, C. Zhang, and J. Gao, “Macrophages as emerging key players in mitochondrial transfers,” *Front. Cell Dev. Biol.* **9**, 747377 (2021).
- ⁶⁷S.-C. J. Hsu, T. U. Luu, T. D. Smith, and W. F. Liu, “Macro- and micro-scale culture environment differentially regulate the effects of crowding on macrophage function,” *Biotechnol. Bioeng.* **121**(1), 306–316 (2024).
- ⁶⁸J.-C. Tardif, S. Kouz, D. D. Waters, O. F. Bertrand, R. Diaz, A. P. Maggioni, F. J. Pinto, R. Ibrahim, H. Gamra, G. S. Kiwan, C. Berry, J. López-Sendón, P. Ostadal, W. Koenig, D. Angoulvant, J. C. Grégoire, M.-A. Lavoie, M.-P. Dubé, D. Rhainds, M. Provencher, L. Blondeau, A. Orfanos, P. L. L’Allier, M.-C. Guertin, and F. Roubille, “Efficacy and safety of low-dose colchicine after myocardial infarction,” *N. Engl. J. Med.*, **381**(26), 2497–2505 (2019).
- ⁶⁹N. Bouabdallaoui, J.-C. Tardif, D. D. Waters, F. J. Pinto, A. P. Maggioni, R. Diaz, C. Berry, W. Koenig, J. Lopez-Sendon, H. Gamra, G. S. Kiwan, L. Blondeau, A. Orfanos, R. Ibrahim, J. C. Grégoire, M.-P. Dubé, M. Samuel, O. Morel, P. Lim, O. F. Bertrand, S. Kouz, M.-C. Guertin, P. L. L’Allier, and F. Roubille, “Time-to-treatment initiation of colchicine and cardiovascular outcomes after myocardial infarction in the Colchicine Cardiovascular Outcomes Trial (COLCOT),” *Eur. Heart J.* **41**(42), 4092–4099 (2020).
- ⁷⁰N. K. Drew, N. E. Johnsen, J. Q. Core, and A. Grosberg, “Multiscale characterization of engineered cardiac tissue architecture,” *J. Biomech. Eng.* **138**(11), 1110031–1110038 (2016).
- ⁷¹M. Mehrabi, T. A. Morris, Z. Cang, C. H. H. Nguyen, Y. Sha, M. N. Asad, N. Khachikyan, T. L. Greene, D. M. Becker, Q. Nie, M. V. Zaragoza, and A. Grosberg, “A study of gene expression, structure, and contractility of iPSC-derived cardiac myocytes from a family with heart disease due to LMNA mutation,” *Ann. Biomed. Eng.* **49**(12), 3524–3539 (2021).
- ⁷²J. Q. Core, M. Mehrabi, Z. R. Robinson, A. R. Ochs, L. A. McCarthy, M. V. Zaragoza, and A. Grosberg, “Age of heart disease presentation and dysmorphic nuclei in patients with LMNA mutations,” *PLoS One* **12**(11), e0188256 (2017).
- ⁷³S. P. Sheehy, F. Pasqualini, A. Grosberg, S. J. Park, Y. Aratyn-Schaus, and K. K. Parker, “Quality metrics for stem cell-derived cardiac myocytes,” *Stem Cell Rep.* **2**(3), 282–294 (2014).
- ⁷⁴R. D. H. Tran, T. A. Morris, D. Gonzalez, A. H. S. H. A. Hetta, and A. Grosberg, “Quantitative evaluation of cardiac cell interactions and responses to cyclic strain,” *Cells*, **10**(11), 3199 (2021).
- ⁷⁵F. Meng and C. A. Lowell, “Lipopolysaccharide (LPS)-induced macrophage activation and signal transduction in the absence of Src-family kinases Hck, Fgr, and Lyn,” *J. Exp. Med.* **185**(9), 1661–1670 (1997).
- ⁷⁶F. Y. McWhorter, T. Wang, P. Nguyen, T. Chung, and W. F. Liu, “Modulation of macrophage phenotype by cell shape,” *Proc. Nat. Acad. Sci. U. S. A.* **110**(43), 17253–17258 (2013).
- ⁷⁷V. S. Meli, H. Atcha, P. K. Veerasubramanian, R. R. Nagalla, T. U. Luu, E. Y. Chen, C. F. Guerrero-Juarez, K. Yamaga, W. Pandori, J. Y. Hsieh, T. L. Downing, D. A. Fruman, M. B. Lodoen, M. V. Plikus, W. Wang, and W. F. Liu, “YAP-mediated mechanotransduction tunes the macrophage inflammatory response,” *Sci. Adv.* **6**(49), eabb8471 (2020).
- ⁷⁸D. L. M. Hickson-Bick, C. Jones, and L. M. Buja, “The response of neonatal rat ventricular myocytes to lipopolysaccharide-induced stress,” *Shock* **25**(5), 546–552 (2006).
- ⁷⁹J. Chen, Q. Ma, J. S. King, Y. Sun, B. Xu, X. Zhang, S. Zohrabian, H. Guo, W. Cai, G. Li, I. Bruno, J. P. Cooke, C. Wang, M. Kontaridis, D.-Z. Wang, H. Luo, W. T. Pu, and Z. Lin, “aYAP modRNA reduces cardiac inflammation and hypertrophy in a murine ischemia-reperfusion model,” *Life Sci. Alliance* **3**(1), e201900424 (2019).
- ⁸⁰A. Grosberg, P.-L. Kuo, C.-L. Guo, N. A. Geisse, M.-A. Bray, W. J. Adams, S. P. Sheehy, and K. K. Parker, “Self-organization of muscle cell structure and function,” *PLoS Comput. Biol.* **7**(2), e1001088 (2011).
- ⁸¹A. R. Ochs, M. Mehrabi, D. Becker, M. N. Asad, J. Zhao, M. V. Zaragoza, and A. Grosberg, “Databases to efficiently manage medium sized, low velocity, multidimensional data in tissue engineering,” *J. Visualized Exp.* **2019**(153), e60038.
- ⁸²A. A. Schmidt and A. Grosberg (2025). “Data from: Polarized macrophages modulate cardiac structure and contractility under hypoxia in novel immunohart on a chip,” Dryad. <https://doi.org/10.5061/dryad.0k6djhbc7>